Charge converters

Semiconductor detectors, high-pressure xenon gas detectors in computer tomographs, xeroradiography:

The electron-hole pairs or electron-ion pairs created by the fast electrons are separated by an external field and the current pulse is used to make a measurement. In xeroradiography a surface charge relief is produced.

Luminescence

Fluorescent screens for cassette recording and image intensifiers, Anger cameras, detectors in computer tomographs.

The fast electrons knock electrons in the crystal out of the valence band into the conduction band; the rule of thumb is that one needs on average three times the energy of the band gap for each pair production (electron/hole). The electrons can then either recombine directly with their hole (crystal luminescence), or they can diffuse to the bottom edge of the conduction band and return from there via the electron traps back to the valence band. Of course, some of the electrons may also recombine without emitting radiation, e.g. where there are defects in the crystal.

4 X-ray computed tomography

4.1 Principles of computed tomography

4.1.1 Introduction

Computed tomography is a special x-ray tomography method which is fundamentally different from the classical x-ray tomography method based on the blurring principle [4.1], in the way the image is formed. It is not absolutely essential to use a computer in order to carry out the method, so that the name computed tomography is actually misleading. However, the use of a computer to produce the images has proved to be extremely useful.

The method produces axial transverse tomograms, i.e. images of body layers which are essentially perpendicular to the longitudinal axis of the body. Although layers with corresponding orientation can be obtained using the classical photographic axial transverse tomography method [4.2, 4.3], these images usually have poor contrast. A large number of attemps have therefore been made to generate x-ray transaxial tomograms with better quality ([4.4], [4.5], [4.6]). In 1963 and 1964, A.M. Cormack was the first to describe an x-ray tomography method completely corresponding to computed tomography which made it possible to produce an image of a layer from a large number of lateral sections determined by x-ray techniques. It was subsequently discovered that the mathematical solution of this problem had already been given by Radon [4.9] in 1917. The first clinical application of computed tomography then followed in 1972 by Hounsfield [4.10] and Ambrose [4.11].

Classical x-ray techniques always produce a photographic recording of the two-dimensional shadow image of the three-dimensional object area projected by the radiation cone into the image plane. In images produced in this way, structures are necessarily superimposed from different object depths. Here, classical survey exposures or spot exposures can only be distinguished from classical tomograms by the fact that in the former the structures from different object depths have equally sharp images apart from small differences due to the radiation geometry whereas in the latter, with the exception of the structures in the layer concerned, the structures have more or less blurred images.

Computed tomography, however, avoids this superposition effect by only processing information on the layer, i.e. slice, of interest to the image. Thus, in the computer tomogram, an object detail exactly corresponds to an image detail and not to a large number of object elements lying behind each other in the

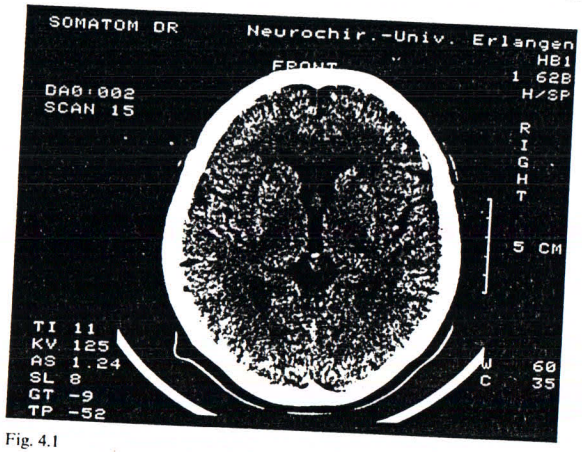

Fig. 4.1
Computer tomogram of a skull. The photograph shows a section at the height of the ventricles which can be easily distinguished from the cerebral matter without any contrast agent. White and gray cerebral matter can be distinguished in this image. Because of its high fat content, the white matter appears darker, i.e. with lower attenuation capacity than the gray matter

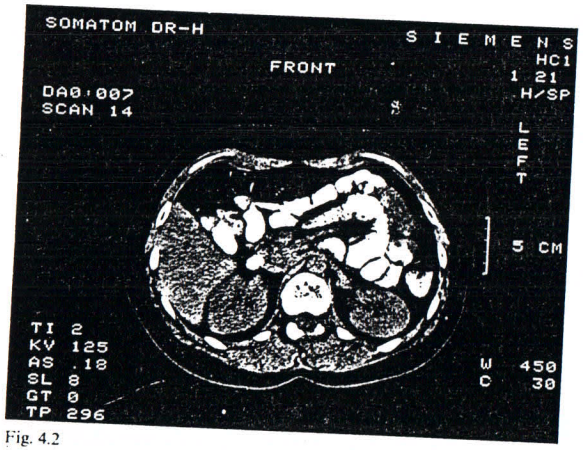

Fig. 4.2
Computer tomogram of an abdomen. The liver, kidneys, aorta, muscles and a large number of other details are clearly demarcated in this tomogram. Their different attenuation capacities can easily be seen

direction of radiation. Such an image which is free of superpositioning is called a substitution image. The capacity of computer tomographs to produce a substitution image instead of a superposition image is one of the main reasons for the high effectiveness of the method: computed tomography provides soft-tissue images with extremely high contrast, which cannot be achieved by classical methods. In addition, because of the special type of image generation, it produces images which can even be evaluated quantitatively.

As a result of these outstanding properties, computed tomography, only a few years after its introduction, has already established itself as an indispensable standard technique, at least in the field of neuroradiology (Fig. 4.1), but also in the radiological examination of other body areas (Fig. 4.2). Its scope of applications is constantly being widened.

In a large number of cases, the high-contrast soft-tissue images which can be obtained make it possible to image structures directly without using a contrast medium. For example, computed tomography enables the cerebral ventricles to be shown directly, so that the number of pneumoencephalograms has been considerably lowered through the introduction of this new technique. Frequently, an injection of contrast medium into the bloodstream can also be avoided. At least high-risk intraarterial contrast administration can be replaced by low-risk intravenous contrast administration. Here, the special advantage of the new imaging technique is not just in the reduction of the risk of a contrast agent accident, but in particular in the reproduction of the actual shape of the organs or lesions: conventional angiography often only produces indirect information, e.g. through vessel displacement. Although computed tomography does not make angiographic examination methods obsolete, it does provide in many cases a more rigorous indication for angiography.

The quantitative nature of the computer tomogram opens up completely new possibilities for image evaluation. However, we will not look at this any more closely here, since it will be treated in depth in section 8.2.

4.1.2 Basic principle

The most important components of a computer tomograph and their operation are shown in the form of a block diagram in Fig. 4.3. In order to generate an image of the body slice of interest, the attenuation of radiation by the object is determined for a large number of paths through the object slice by means of a measurement arrangement consisting of an x-ray tube and a radiation detector system. The simplest form of measurement system, shown in Fig. 4.3, uses an x-ray beam about the thickness of a pencil passing through the slice for measuring the attenuation. The attenuation is determined by first moving the measurement system perpendicular to this beam and parallel to the slice plane over the entire object cross-section. At the same time, the radiation intensi-

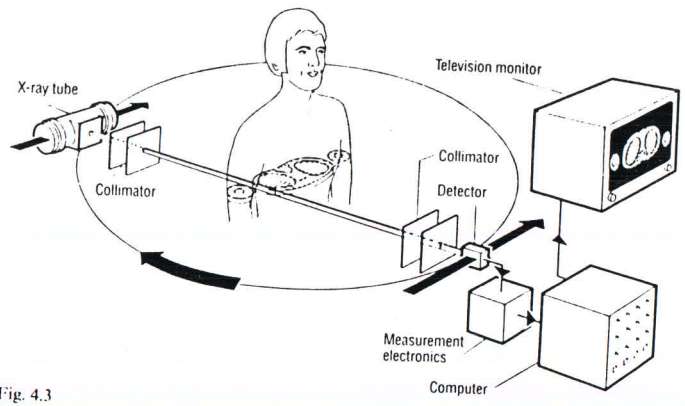

Fig. 4.3
Basic representation of a computer tomograph in the simplest design form. The measurement system, consisting of x-ray tube and radiation detector, is first moved linearly in the slice plane over the entire object cross section. The measurement system is then rotated about approximately 1° and then a new linear scanning movement performed, etc., until an angle of at least 180° has been traversed. Throughout the entire scanning process, the measurement signal obtained by an x-ray beam approximately the thickness of a pencil is recorded at fixed intervals and transferred to a computer. This computes a two-dimensional distribution of attenuation values corresponding to the object layer from the measurement values, which is finally displayed as a tomogram on a television monitor after conversion to video signals

ty at the detector is recorded at fixed predetermined intervals, so that an initial set of measurement values is obtained which corresponds to a lateral section of the slice and is called a projection. In contrast to classical x-ray technology, a large number of such projections is needed in computed tomography to generate an image. They are obtained by rotating the measurement system through a small angle of 1° about the system axis perpendicular to the slice plane after one projection is measured and then initiating another linear scanning process, etc., until the measurement system has traversed an angle of rotation of at least 180°. During the measurement process, the measurement values are coded in suitable form and transferred to a computer. With the present state of the art, every image requires a few hundred projections and every projection

a few hundred measurement values, so that in total about 100000 to 1000000 measurement values are involved. The computer then calculates from all these measurement values a two-dimensional attenuation distribution corresponding to the object as an image of the slice, where object areas with high attenuation are assigned high numerical values and object areas with low attenuation are assigned low numerical values. Since the computer, just as it can only process a finite number of measurement values, can only calculate a finite number of attenuation values, the object slice must be thought of as divided into small volume elements ("voxels") with a square base, inside which the attenuation value is assumed to be constant (Fig. 4.4) and is then calculated by the computer. However, in practice the attenuation value of the object material will usually vary inside the individual layer elements, so that the calculated attenuation value is always obtained as an average over the volume element concerned. This should always be borne in mind, in particular in quantitative image evaluation.

At first, the slice image is only present in the computer in the form of a stored set of numbers and is thus not immediately accessible. The simplest way to make the image accessible to the eye is to print the attenuation values in an arrangement corresponding to the position of the volume elements assigned to them in the object layer. However, the visual evaluation of such an arrangement of numbers, also called a matrix, proves to be very laborious, especially because of the large number of matrix elements, which at present usually lies between 256 × 256 and 512 × 512. This image representation method is therefore only used in rare cases and then mostly only for parts of the image. Usually, the numerical matrix is converted into a black and white or color television image in which each image point ("pixel") corresponds to a matrix element and different gray or color tones are assigned to the different attenuation values.

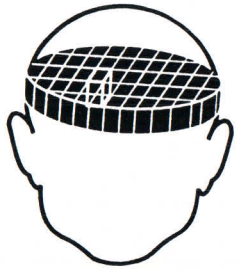

Fig. 4.4
Decomposition of the object slice into volume elements. The object layer is considered as made up of a large number of such small volume elements with a square base. The attenuation capacity of the object material is assumed to be constant inside these elements

4.1.3 Attenuation scale

For the attenuation of a monochromatic x-ray beam passing through a homogeneous material, we have

$$J = J_0 e^{-\mu x} \tag{4.1}$$

where

J is the radiation intensity behind the object
J_0 is the radiation intensity at the same point in the absence of the object
x is the object thickness
μ is the linear attenuation coefficient of the material for the radiation used.

The value of μ strongly depends on the radiation energy and is therefore only of limited use for characterizing the radiation attenuation capacity of an object in computed tomography, since it would only be possible to compare the results obtained with different equipment if all these different types of equipment were to use exactly the same radiation. This is why in computed tomography an

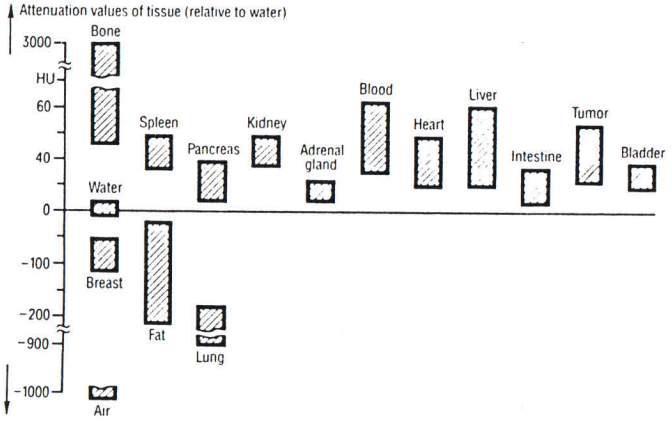

Fig. 4.5
Attenuation value ranges of different body substances and tissues. It can be seen that the attenuation value ranges corresponding to the individual substances frequently overlap. Therefore, it is not possible to unambiguously identify the substance from the attenuation value. This applies, in particular, to the different types of tumors

attenuation value is used which is the scaled relative deviation of the linear attenuation coefficient of the investigated object from the linear attenuation coefficient of a generally available reference material similar to the object. In practice, water is used as the reference material. The attenuation value is therefore given as

$$\mu_{rel} = k \frac{\mu_{object} - \mu_{H_2O}}{\mu_{H_2O}}. \tag{4.2}$$

As a rule, the factor k is chosen as 1000, so that in this scale water has the attenuation value 0 and air -1000, whereas very dense bone tissue lies around $+3000$ because its linear attenuation coefficient for the radiation energy values used in computed tomography is approximately four times that of water. The position of other tissue types on this scale is shown in Fig. 4.5.

4.1.4 Image generation

In order to construct a usable tomogram from the measured intensity profiles, a simple computational superposition of the individual intensity signals corresponding to the projection direction in the image matrix is inadequate (Fig. 4.6). Instead, the measured intensity J has to be converted to the quotient of the intensity J_0 (without attenuating medium) and J and then the logarithm of this quotient taken. In this way, values proportional to the linear attenuation coefficient of the object material are obtained before superposition. By taking the logarithms of both sides and rearranging, from the attenuation law – equation (4.1) – we obtain:

$$\mu = \frac{1}{x} \ln \frac{J_0}{J}. \tag{4.3}$$

However, even a superposition of the projections preprocessed in this manner still does not give us the required result. Such an image exhibits extensive blurring (Fig. 4.6a). In order to avoid such blurring, the preprocessed projections are convoluted with a filter function before superposition (Fig. 4.6b). Because of this preprocessing step, the entire image generation process described here, which is commonly used today in computed tomography, is called the convolution process. This convolution results in modified signals, which contain negative as well as positive components. If the filter function is suitably chosen, they have the properties that when the convoluted projections are superimposed, this extensive blurring is exactly cancelled out. One consequence of this convolution process and subsequent projection superposition is that every measurement

value makes a contribution to every image point, even though with very different weighting. This is of special importance for the artifact behavior of computed tomography, which is completely different from classical x-ray techniques.

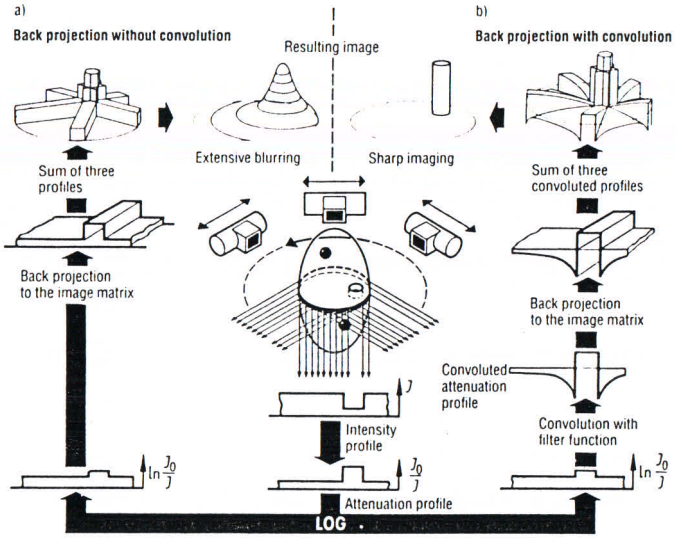

Fig. 4.6
Importance of convolution for image reconstruction in computed tomography. The intensity profiles J obtained by measurement are converted to attenuation profiles J_0/J, where J_0 is the intensity measured without the object in the radiation path. The attenuation profiles are then converted to logarithms, so that a quantity proportional to the attenuation coefficient is available for further processing. If, as shown in path a, the logarithmic attenuation profile is simply superimposed according to its projection direction, then there would be considerable blurring of the detail to be imaged. Therefore, in computed tomography, there is a specific alteration of the logarithmic attenuation profile, as shown in path b, by convolution with a suitable filter function. The convoluted profiles exhibit negative as well as positive components, whose contributions to the superposition image exactly cancel the extensive blurring when the filter function is correctly chosen

4.1.5 Types and properties of equipment

Since the introduction of computed tomography, considerable effort has been made to improve the effectiveness of the equipment, in particular to cut down the imaging time. This has led to the development of different scanning systems, which essentially differ in terms of the number and arrangement of the detectors. As the following comparison shows, each of the individual systems has certain advantages which are always offset by certain disadvantages.

The measurement system already mentioned, shown again in Fig. 4.7a with a single radiation beam of pencil thickness, is in fact the arrangement which is least commonly used for attenuation measurement: it only utilizes a vanishingly small fraction of the radiation generated in the x-ray tube. While the radiation released at the anode of the x-ray tube is emitted into all of the half space, i.e. a solid angle of $2\pi = 6.28$ radians, the radiation beam which is finally used for measurement only takes up a solid angle of approximately 10^{-4} radians. Since, on the one hand, the power of an x-ray tube is limited and, on the other hand, a certain amount of radiation (dose) is needed to produce a usable computer tomogram, and in addition the machine cannot be moved at unlimited speed, such a measurement system requires relatively long exposure times of the order of magnitude of a few minutes; it is therefore only suitable for the examination of stationary parts of the body or areas of the body which are easy to keep still, in particular for skull examinations.

The total examination time can be reduced by using a second detector directly following the first detector in the direction of the layer thickness, otherwise keeping the same geometrical relationships, collimating the radiation beam correspondingly to both detectors and so processing the measurement data for two immediately adjacent slices at the same time. However, a real reduction in the exposure time for the same dose can only be achieved through increasing the number of measurement channels per layer by arranging several detectors next to each other in the scanning direction as is shown for example in Fig. 4.7b and collimating the beam at the x-ray tube to a fan shape. With such a measurement arrangement, utilizing the radiation generated in the x-ray tube in a much better way, it is possible to obtain the measurement data for a number of projections corresponding to the number of detectors at the same time, so that the system rotation angle between two linear scanning processes can be increased and thus the number of linear scanning processes and rotation steps decreased. Measurement times achieved with such equipment lie between 10 and 60 seconds, depending on the number of detectors per slice. However, there is a limit to any further reduction in the measurement time in these measurement systems for mechanical reasons, because of the alternating sequence of translational and rotational motions.

The shortest exposure times, of the order of a few seconds, can be obtained by using an x-ray fan covering the entire object cross-section in conjunction

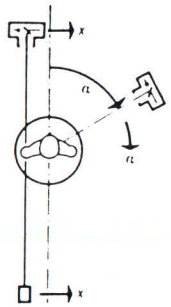

a) The parallel-beam system with only one measurement beam (see also Fig. 4.3), alternately moved in a translational and rotational manner, only poorly utilizes the radiation of the x-ray tube and requires a long measuring time

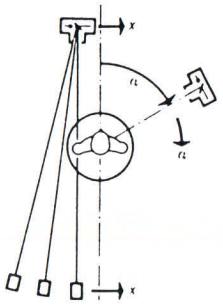

b) The parallel-beam system with several measurement beams makes better use of the generated radiation, reduces the number of movement steps and therefore cuts down the measurement time

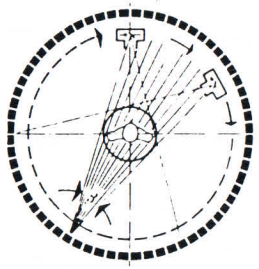

c) The ring-detector system has a fixed detector ring, operates with a fan-shaped x-ray beam simultaneously covering the entire patient cross section and therefore only requires a rotational movement of the x-ray tube

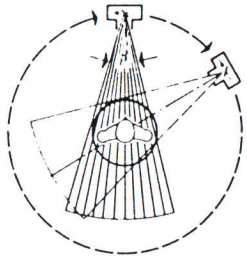

d) The fan-beam system has a multicellular detector system rotating about the patient together with the x-ray tube

Fig. 4.7
Scanning principles of different computed tomography systems

with a corresponding multi-cellular detector system. In this case, the radiation generated in the tube is optimally utilized and in addition it is only necessary for the system to execute purely rotational movements, which do not have to be in steps but can be performed continuously. Two different detector arrangements are possible, as shown in Figs. 4.7c and 4.7d: either a detector system which moves around the patient together with the tube or a stationary detector ring. In the case of the travelling detector system, the radiation is either switched on in pulses at fixed angular intervals or continuous radiation is used and the detectors are switched on and off. Only the second operating principle is common in equipment with a detector ring.

In contrast to translation-rotation systems, which always produce sets of measurement data for parallel projections and are therefore also called parallel beam scanners, in purely rotational systems primary sets of data are produced which correspond to central projections. Whereas in the case of a detector system moving together with the x-ray tube the projection center is always the tube focus (fan-beam scanner), in the case of a stationary detector ring, the individual detectors can also be interpreted as projection centers (ring-detector scanner), which is also usually the case in the corresponding equipment design.

It will be shown in Section 4.2 that a computer tomogram can be constructed directly from parallel projections as well as from central projections. However, since the amount of computation is greater in the latter case, in some types of equipment the sets of measurement data originally obtained as central projections are first rearranged to parallel projections before the actual reconstruction of the computer tomogram. In this case, though, it is no longer possible to process the measurement data in step with the data acquisition process, since all measurement data have to be collected first prior to complete rearrangement.

The reduction in scan time obtained by successively increasing the measurement beam in various scanning systems is offset by an increased level of scattered radiation at the detector entrance. Particularly with fan-beam equipment and ring detector equipment, which both operate with fan beams covering the entire cross section of the patient, it is necessary to reduce the amount of scattered radiation among the radiation which reaches the detector system. In fan-beam equipment, it is relatively easy to do this by installing an anti-scatter collimator focussed on the focal spot of the x-ray tube in front of the detector system. This collimator then rotates around the patient together with the measurement system (Fig. 4.8a). However, for ring detector equipment with the usual radiation geometry, as shown in Fig. 5.7c, it is not possible to have a fixed anti-scatter collimator in front of the detector system because this could only be focussed on the center of rotation and not on the focal spot (Fig. 4.8b). Instead, it would be necessary to provide a collimator with moving lamellae which would always have to be pointing at the focal spot. This is only possible by means of a complicated and very precisely operating mechanism. Since this is hardly feasible, the distance between patient and detector is chosen as large as possible,

as in the well-known Groedel technique for classical radiography [4.12], in order to reduce the amount of scattered radiation in the signal which reaches the ring-detector equipment. However, in view of the equipment dimensions which are possible, the scattered radiation cannot be suppressed as drastically as by means of a collimator.

Apart from the various problems arising from scattered radiation, there are other important differences between the individual measurement arrangements in terms of image quality and image characteristics. These affect, for instance, the geometrical resolution and the image noise. In this respect, parallel-beam and ring-detector scanners behave in practically the same manner, because their scanning principles differ only slightly, whereas there are marked differences between these systems on the one hand and fan-beam scanners on the other hand.

For parallel-beam and ring-detector scanners, the linear distance or the angular distance of the individual measurement beams within a projection can be chosen independently of the width of the individual measurement beams in the scanning direction. On the other hand, for fan-beam scanners, the distance and the width of the individual measurement beams are fixed by the detector arrangement (Fig. 4.9). Since the measurement beam width b and the center-to-center distance a of the measurement beam components determine the spatial resolution d of the system according to the relationship

$$d = \sqrt{a^2 + b^2} \tag{4.4}$$

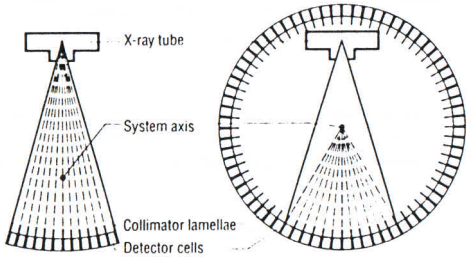

a) Fan-beam scanner b) Ring-detector scanner

Fig. 4.8
Possibilities for eliminating scattered radiation by a lamellar collimator connected to the detector system. For the fan-beam scanner (a) it is easily possible to insert a rigid anti-scatter collimator, focussed on the focal spot of the x-ray tube and attached to the detector system. For the ring-detector scanner in the usual arrangement (b), on the other hand, a rigid collimator could only be focussed on the center of rotation, so that shadows would be formed of the primary radiation towards the edge of the fan. In this case, the collimator lamellae would have to be moveable and would have to be kept pointed to the focal spot of the tube by a tracking mechanism

and the distance a fixes the noise-grain size in the reconstructed image. This means that, in contrast to fan-beam scanners, by means of a suitable choice of the distance a in parallel-beam and ring-detector scanners, the noise-grain size can to a large extent be selected independently of the spatial resolution. In another type of equipment, with fan-beam and flying focal spot, the focus is approximately fixed in space by periodic electron beam deflection for the duration of each readout cycle, whereas the fan-beams, due to the continuous detector movement A_D at the center of rotation, perform a swinging movement a about the focus (Fig. 4.9c). During this movement, n readouts can be made at the beam center distance a/n, as if the detector had an n times finer partitioning. This considerably increases the resolution, with the radiation beam width b remaining the same.

For parallel-beam, ring-detector and flying focal spot scanners, apart from the detector and focal spot width, the movement of the measurement beam influences the effective measurement beam width and thus also the geometrical resolution during a measurement interval. As shown in Fig. 4.10, this is not the case for conventional fan-beam scanners.

For a given image matrix, it is no longer possible to achieve any noticeable improvement in the image quality through increasing the number of measurement values in each projection and the number of projections above a certain

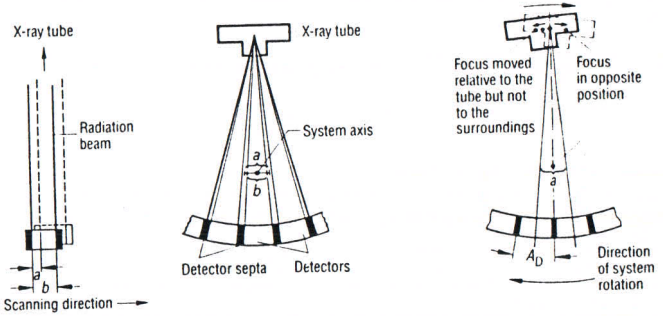

a) Parallel-beam scanner b) Fan-beam scanner c) Fan-beam scanner with flying focal spot

Fig. 4.9
Relationship between the measurement beam width and distance for different scanning systems. For parallel-beam systems (a), ring-detector systems and systems with flying focal spot (c), the center-to-center distance a of the individual measurement beams can be chosen independently of their width b by fixing the number of measurements. For fan-beam systems (b), the center-to-center distance a of the individual measurement beams is always greater than the measurement beam width b, because of gaps between the beam segments dictated by design

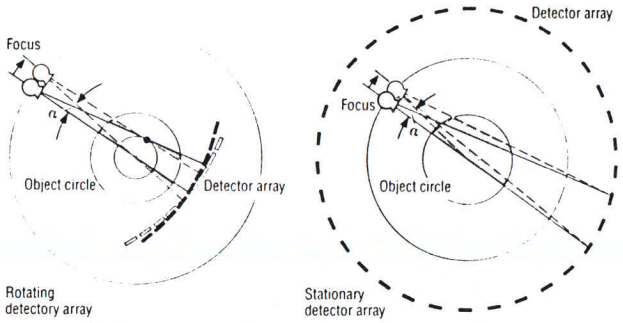

a) Fan-beam scanner b) Ring-detector scanner

Fig. 4.10
Effect of movement of the focal spot on the measurement beam width for different scanning systems. For conventional fan-beam systems (a) the focal spot and detector move together around the object, so that there is no blurring, i.e. broadening of the measurement beam, and thus no reduction in the geometrical resolution due to movement of the measurement system during the measurement process at the center of the image. However, in the ring-detector system (b), movement of the focus also produces such a blurring at the center of the image. The same applies to parallel-beam systems and flying focal spot systems

value. This results in a particular disadvantage of ring-detector scanners compared to fan-beam scanners in terms of the geometrical resolution: because of the high costs entailed, every effort is made to keep the number of detectors and measurement channels as small as possible to satisfy the specifications of image quality. Due to the equipment dimensions determined by the object sizes, this results in a relatively large detector distance for ring-detector systems compared with fan-beam systems having the same number of projections and thus a correspondingly large detector width, if the radiation in the detector plane is to be well utilized. However, the large detector width likewise leads to a relatively large measurement beam width and in turn to a correspondingly lower spatial resolution.

With some parallel-beam and ring-detector scanners, it is possible to reduce the detector width by additional collimation and thus increase the spatial resolution. However, in this case the radiation arriving in the detector plane is only partly utilized. This leads to higher image noise and thus also to a lower density resolution capacity for the same dose in the detector plane, which therefore indirectly means an increase in the radiation received by the patient.

The characteristics described above by no means cover all the differences between the various scanning systems. However, the comparison already makes

it quite clear that every system has advantages and disadvantages, so that no single system can be regarded as optimal. The required image quality, costs and application determine which type of equipment is the best in each individual case.

4.1.6 Beam quality and measurement value corrections

Ideal measurement conditions would be present if it were possible to measure the radiation attenuation with monochromatic radiation, i.e. with radiation which only consists of quanta having the same energy (Fig. 4.11 a). In this case, practically only radioactive isotopes could be considered as a radiation source. However, there is no isotope which can emit a quantum energy suitable for computed tomography (60 – 80 keV) and which can be produced with sufficiently high specific activity to make sufficiently small sources available with adequate radiation intensity. Therefore, apart from special equipment for small object diameters, one is forced to use an x-ray tube as a radiation source for computer tomographs. However, the anode of an x-ray tube emits x-ray quanta with an energy varying from a few keV to a maximum energy of the order of 100 to 150 keV, depending on the voltage applied to the tube. A typical radiation spectrum of an x-ray tube for computed tomography is shown in Figs. 4.11 b and 4.11 c.

As they pass through the object, the various spectral components of the beam undergo very different attenuation, so that the attenuation law in the simple form of relationship (4.1) can only be applied to the individual energy components. In fact, for a homogeneous material, one measures

$$J = \int J_0(E)\, e^{-\mu(E)x}\, dE \tag{4.5}$$

and for an inhomogeneous material, one measures

$$J = \int J_0(E)\, e^{-\int \mu(x,E)\, dx}\, dE, \tag{4.6}$$

where J_0 and μ depend on the quantum energy E and μ also depends on the position x along the measurement beam. No account has been taken here of the fact that the sensitivity of the detector system can also vary for the different spectral components.

The energy composition of the beam after passing through an object of given material, e.g. water, therefore depends on the object thickness (Fig. 4.11 b). In other words, the linear attenuation coefficient determined by (4.1) for the same material varies with the object thickness in such a way that it decreases with increasing object thickness. The lower energy soft radiation components are more strongly attenuated than the higher energy hard components, so that the mean energy of the radiation spectrum is shifted to higher energies after

passing through an attenuating medium. This process is called hardening. A result of the hardening effect is that, for example, the measurement of a homogeneous object with elliptical cross-section gives a different attenuation coefficient in the direction of the minor semi-axis than in the direction of the major semi-axis. The results of the two measurements are therefore inconsistent and they must be brought into agreement by suitable measures before image reconstruction. A first step is to confine the spectral distribution by suitable prefiltering of the radiation. This removes the soft radiation components, which can only penetrate the object to a small extent and therefore only contribute to the radiation exposure of the patient without contributing to the signal intensity at the detector.

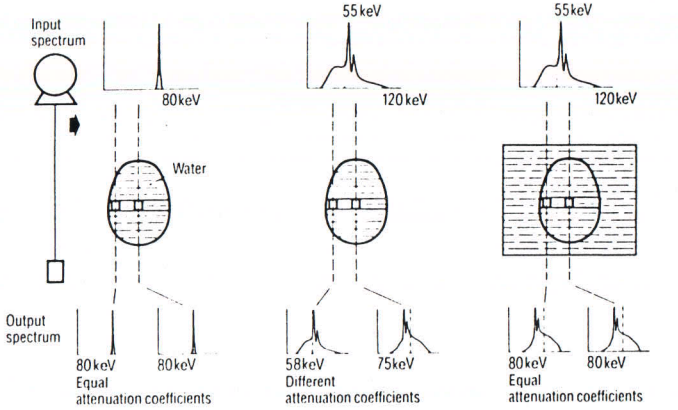

a) Monochromatic radiation

b) Radiation of an x-ray tube without compensation body

c) Radiation of an x-ray tube with compensation body

Fig. 4.11
Beam hardening and compensation body. Monochromatic radiation (a) would allow ideal measurement conditions. The measured radiation spectrum would be independent of the composition and thickness of the object. However, the radiation spectrum of an x-ray tube used in practice (b) covers a relatively large energy range. The soft spectral components are attenuated more strongly than the hard spectral components. This shifts the mean energy value of the spectrum to higher energy values when the radiation passes through the object: the radiation becomes harder. For one and the same material, we therefore have a different attenuation value for every material thickness without appropriate correction. By embedding the object in a compensation body (c) made of material similar to the object, effects of beam hardening, which are different for different object regions, can be reduced considerably

However, prefiltering is not sufficient to reduce the beam hardening effect to an insignificant level. Therefore, in the first computer tomographs, the object was embedded in a compensation medium of a material similar to the object (water and suitable plastics) to ensure that the path length of the radiation in the attenuating medium was the same in all directions, so that the signal changes at the detector were only caused by the small material and density differences in the object (Fig. 4.11c). This type of correction was entirely sufficient and, in addition, ensured that the signal range at the detector was reduced to a minimum. It therefore contributed considerable advantages to the design of the detectors and associated measurement electronics. However, the compensation medium was a source of discomfort for the patient, caused problems in the examination of casualty patients and could only be offered at considerable costs for parts of the body with large variations in diameter (thorax and abdomen). This means of beam hardening correction was therefore very soon re-

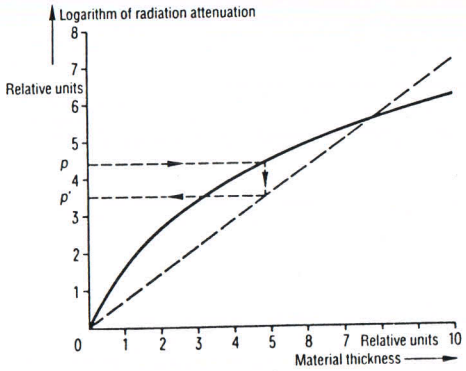

Fig. 4.12
Correction for beam hardening without compensation body. With the radiation quality chosen for the patient scans, the logarithm of the radiation attenuation is determined experimentally by measuring slices of different thickness of a material as similar as possible to the body. This generally gives a relationship such as shown by the solid curve. However, with no beam hardening effects, a straight line should be produced. We therefore choose a reference point on the measured curve and draw the dotted line through this point and the coordinate origin, which represents the required linear relationship between the material thickness and the logarithm of the attenuation. The corrected value p' corresponding to a measured value p of the logarithm of the attenuation is found by determining the material thickness associated with p on the measured curve and then reading off the value p' of the logarithm of the attenuation assigned to this material thickness from the straight line. In the computer, this correction process can be performed by accessing appropriate tables

placed by purely computational signal correction, although this considerably increased the costs of the measurement electronics because of the vastly greater signal range at the detector. In order to provide the basis for purely computational beam hardening corrections, the attenuations J_0/J are determined for different material thicknesses of a substance as similar to the body as possible, e.g. water (Fig. 4.12). The logarithms of these values would be linearly dependent of the layer thickness if there were no beam hardening. In practice, though, we do not obtain a straight line. We therefore choose a point on the curve, i.e. a specific material thickness, and draw a straight line between the coordinate origin and this point. The image reconstruction is then based on the corrected value of the layer thickness read from this straight line instead of the measured values lying on the curve. In the computer, this correction is carried out either by using look-up tables or by using a suitable approximation function.

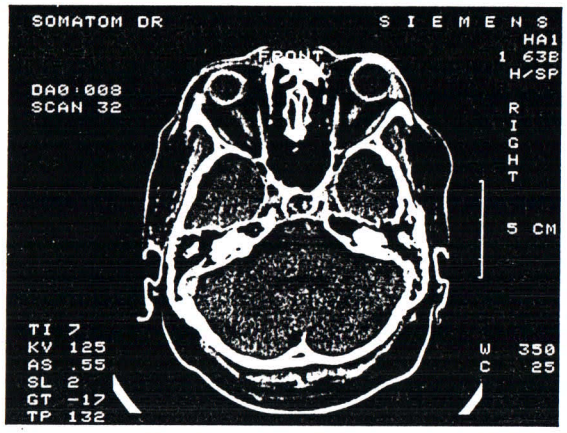

Fig. 4.13
Limits to the beam hardening correction. A beam hardening correction determined with, for example, material equivalent to soft tissue will only have an incomplete effect as soon as more extensive object structures occur in the slice under examination, for which the energy dependence of their attenuation capacity is different than that of soft tissue. This skull tomogram shows a typical artifact in the center of the image: a broad soft tissue band of apparently reduced attenuation capacity. This soft tissue area is reproduced with incorrect attenuation values since the extensive neighboring bone structures (petrous bones) have completely different beam hardening properties than the soft tissue

Of course, just as with the correction obtained using a compensation medium, this correction is only exact if the object consists entirely of materials which behave in completely the same way as the reference substance in terms of the energy dependence of its radiation attenuation capacity over the range in question. If, for example, water is taken as the reference substance, the correction for soft-tissue components will function very well, but may be inadequate if there is a large amount of bone in the slice. This is the cause of a typical artifact, shown in Fig. 4.13, observed in skull images showing the petrous bones: In a broad band between the petrous bones, the cerebral matter appears darker, i.e. less dense than in the rest of the image. In such a case, it is possible to make use of additional corrections which might possibly be carried out iteratively. These would ultimately produce a perfect reproduction of the morphology and attenuation values, but would also considerably increase the demands on computing resources.

Apart from the correction of the measurement values for the beam hardening effect described in detail above, there are several other corrections which have to be applied to the measurement values before the actual image reconstruction can start. These corrections concern, for example, the individual sensitivity, the offset, the spectral sensitivity distribution and the geometrical arrangement of the individual measurement channels. However, it would go well beyond the scope of this book to give an account of all the corrections which are necessary or conceivable. Further basic considerations on the principles of computed tomography can be found in references [4.13] to [4.19].

4.2 CT image reconstruction

As already explained in detail, x-ray computed tomography (CT) makes it possible to produce radiographical images of transaxial slices of the human body without disturbance due to shadows from adjacent layers. Moreover, in contrast to the classical x-ray image, the CT image is no longer a superposition image. What it reproduces is the local attenuation capacity, i.e. a physical property of the biological tissue, in the form of gray values.

Whereas in classical x-ray tomography, even though a sharp image is produced of one layer, the images of all the layers situated in the radiation paths are superimposed onto the desired layer image with a blurred appearance, in the CT procedure interference shadows arising from structures outside the layer concerned are excluded from the very start. The focal spot and the detector are always situated in the slice plane under investigation; the radiation beam only scans this slice (see Fig. 4.3). On the other hand, this means that every tissue structure in the slice itself produces an interference shadow. In other words, for a predefined position of focal spot and detector, the measured intensi-

ty distribution of the x-rays penetrating the object only provides information on the sum of all attenuations which the x-ray radiation has undergone in the object. The distribution of the attenuation capacity of the tissue along the scan beam cannot be taken from this single measurement value alone. A single projection is therefore not sufficient to determine the distribution of the attenuation capacity in the slice. As can be seen from the example of a parallel-beam scanner in Fig. 4.14, it is still not yet possible to identify tissue structures unambiguously when two mutually perpendicular parallel projections are taken after the manner of the well-known biplane technique in radiography. If, for instance, we replace the four symmetrically arranged rods (Fig. 4.14 left) by two rods of the same thickness with double the attenuation capacity (Fig. 4.14 right), a vertical and a horizontal projection give exactly the same measurement data in both cases: $P_V = P'_V$ and $P_H = P'_H$. Only another projection P_D or P'_D directed

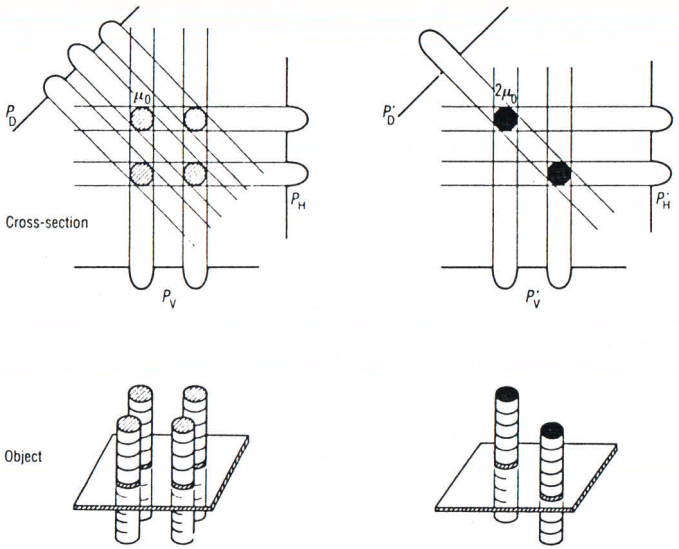

Fig. 4.14
Ambiguity of the scan data: the two rods to be imaged on the right have double the density of the four rods on the left, i.e. $P_H = P'_H$, $P_V = P'_V$. Only an additional diagonal projection P_D or P'_D makes it possible to distinguish between the two structures depicted here

along a diagonal makes it possible to distinguish the two object structures in this case. It is not difficult to imagine that even three projections are not sufficient for the unambiguous identification of more complicated structures. Even if many projections are used, there is always a certain residual uncertainty which increases with increasing fineness of the object structures.

However, objects with arbitrarily fine structure are never imaged in CT, because the effective width of the beam resulting from the detector width, the focus width and the movement of the measurement system – only allows a blurred representation of the object as imaged by the measurement system. In the language of communications theory, the measurement system carries out low-pass filtering and so simulates an object which only contains structures up to a certain level of fineness. Now, a finite number of projections is sufficient in order to unambiguously reconstruct this simulated, blurred image – now free of very fine structures. The question of determining this necessary number of projections will be considered below. The finite detector and focus widths in CT should not just be regarded as an evil, as a cause of the limitation in the resolution, but as a necessary condition for the unambiguous reconstruction of a CT image.

4.2.1 Principles of image reconstruction

The principles of image reconstruction in CT can be explained using the simplest design of a parallel-beam scanner. Fan-beam machines and ring-detector systems require more complicated algorithms, which however can be derived from the algorithms used with parallel-beam systems by a transformation of coordinates. Thus, restricting this discussion to the parallel-beam allows us to focus on the essential details.

This simple scanning principle is shown again in Fig. 4.15. The linear scanning movement takes place for the present in the η direction, characterized by the angle φ. The intensity J measured at the detector therefore depends, on the one hand, on the projection angle φ and, on the other hand, on the position η which the measurement system occupies at any point in time during the scanning movement and of course also on the intensity J_0 of the unattenuated radiation.

$$J = J(\varphi, \eta) = J_0 \, e^{-\int \mu \, d\xi}. \tag{4.7}$$

The path of the given scan beam through the object is taken as the integration path. The distribution of the attenuation coefficient μ in the slice under study can now be calculated from all the measured intensities $J(\varphi, \eta)$. The above integral equation is then solved for μ. However, it is more convenient to first

transform equation (4.7) into a linear integral equation by referring the measured intensity $J(\varphi, \eta)$ to the intensity J_0, which is also known, and taking the logarithm:

$$p_\varphi(\eta) = \ln \frac{J_0}{J(\varphi, \eta)} = \int \mu \, d\xi. \tag{4.8}$$

In many CT systems, this logarithmic approach is already implemented as part of the scan data acquisition, so that the data $p_\varphi(\eta)$ (in digital form) is already transferred to the computer. The calculation of logarithms is therefore considered here as part of the measurement process and the function p_φ is regarded as a projection.

There are two different methods for solving the integral equation (4.8). In one method, it can be immediately written in discrete form, i.e. converted to a linear algebraic equation system which must then be solved. However, closed solution formulae can also be given for equation (4.8). In this case, the transformation to a discrete form is only carried out during the numerical evaluation of the solution formulas.

A minicomputer performs the actual image reconstruction. This computer usually has special arithmetic elements adapted to the requirements of the CT algorithms, permitting extremely fast processing.

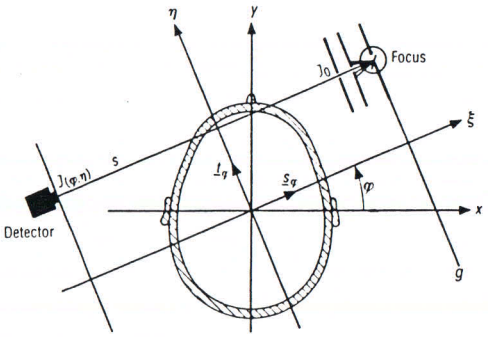

x, y	Coordinates fixed in space
ξ, η	Coordinates bound to the measurement system
φ	Projection angle
s_φ, t_φ	Unit vectors
J	Radiation intensity measured behind the object
J_0	Radiation intensity measured in front of the object

Fig. 4.15 Choice of coordinate systems

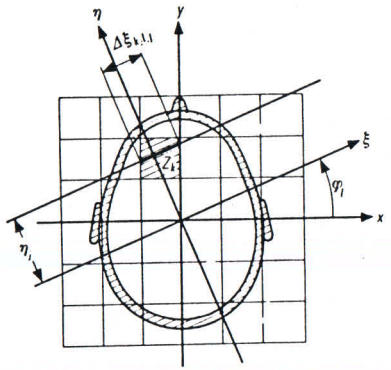

Fig. 4.16
Decomposition of the layer to be imaged into n square cells (pixels)

Z_k	$(1 \le k \le n)$
$\Delta\xi_{k;1,j}$	Radiation path in the cell Z_k

Algebraic reconstruction methods

Historically, algebraic methods are the oldest reconstruction methods in computed tomography [4.20]. Even though there is hardly any likelihood today that they will again supplant the more modern integral transformation methods, they will be briefly described because they provide the simplest and most direct approach to understanding CT image reconstruction.

With these methods, the object is assumed to consist of small square cells (pixels) (Fig. 4.16). This finite number of pixels corresponds to an approximately equal number of measurement data; the linear scanning movements occur with a finite number of equally spaced angles φ_l and for a predefined projection direction φ_l the measured value is determined at a finite number of focus-detector positions η_j.

The measured value $p_{l,j}$, which refers to a scan beam passing through the object, is in this simple model the sum of the μ values of all the pixels encountered by the beam multiplied by the path length $\Delta\xi_{k;l,j}$ which the beam traverses in the cell:

$$P_{l,j} = \sum_k \mu_k \Delta\xi_{k;l,j}. \tag{4.9}$$

This extensive equation system consisting of up to a few hundred thousand variables can in practice only be solved iteratively for reasons of accuracy (rounding off errors!). Here, we will describe the best known iteration method for an extremely simple "object" consisting of four pixels with attenuation values 0.2, 0.3, 0.1 and 0.4 cm^{-1} (Fig. 4.17). (In the following, the unit cm^{-1} will be omitted in describing the attenuation values.)

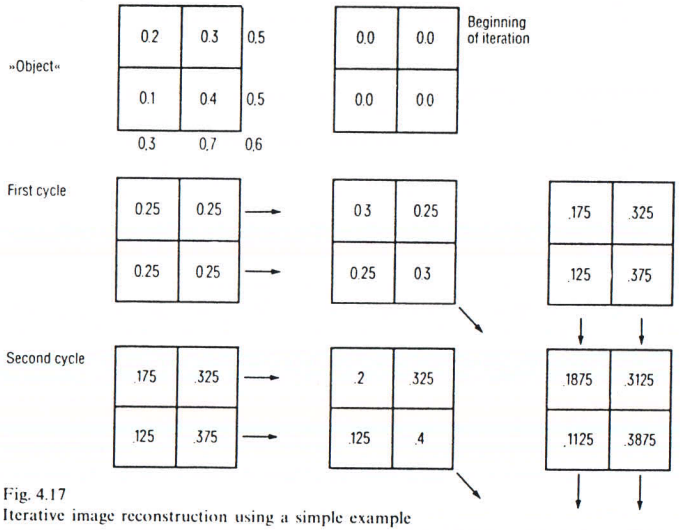

Fig. 4.17
Iterative image reconstruction using a simple example

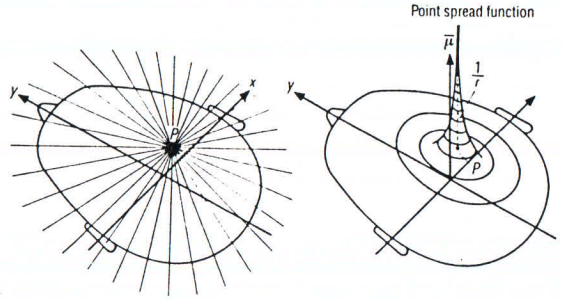

Fig. 4.18
Production of the point image in the form $1/r$ for simple back projection (r is the distance of a predefined point from the object point P)

Starting from the measurement values 0.5 and 0.5, i.e. the measured sums of the attenuation values, all attenuation values are initialized to 0.25 in the first cycle. However, this "image" only satisfies the two "horizontal measurements". The "diagonal measurement" is now satisfied by equally distributing the deviation of the measurement value 0.6 from the measurement value 0.5 which would be obtained if the object actually contained the attenuation values 0.25 and 0.25 along the diagonals, over the two diagonal elements. The two "vertical measurements" are then satisfied, completing an iteration cycle. At this point, the image matrix now no longer satisfies the "horizontal measurement", so that the correction loop has to be repeated until the "image" is finally stabilized.

Integral transformation methods (convolution methods)

Integral transformation methods ([4.21] to [4.25]) are based on solution formulas for equation (4.8) in which only the projections $p_\varphi(\eta)$ still have to be substituted by measurements. Several equivalent methods are available for the theoretical derivation of a solution formula. A particularly easy to visualize approach is the following (Fig. 4.18): we imagine an object which only consists of a single element and which attenuates the x-ray beam. During every linear scanning movement, only a single "measurement beam" is attenuated. Since, however, we now do not know which element on the beam line has caused this attenuation, it is uniformly distributed over the entire line passing through the element, which can be imagined as recorded onto a suitable two-dimensional storage device.

In practice, it is best to use a digital memory whose cell arrangement corresponds to the given division of the image into small pixels in a manner similar to that illustrated in Fig. 4.16.

Every direction, i.e. every angular setting of the scanning arrangement, is treated in the manner described above. The additive superposition of all scan lines then results in a spatial distribution which, as can be immediately seen, falls off from the attenuating object point as $1/r$, where r denotes the distance of a predefined observation point to the object point. By drawing circles of any arbitrary size about this point, there are then always the same number of straight lines uniformly distributed over the circumference of these circles, which increases in proportion to r. In the language of systems theory, we have defined here the point spread function of a linear, position-invariant imaging system, this imaging system consisting of the measurement of the integrals along any arbitrary straight lines and the back projection of the measured values onto the corresponding measurement lines. If, however, the object consists of many x-ray attenuating elements, or to be more exact, of a distribution of μ values, then this imaging system provides such a $1/r$ function for every object point weighted with the local attenuation coefficient. The superposition of all these

functions leads to an approximation image $\tilde{\mu}$, which in the language of mathematics is described as the convolution of the object function μ with the function $1/r$:

$$\tilde{\mu} = \mu * \frac{1}{r}. \tag{4.10}$$

(A dimensional multiplicative constant has been omitted here.)

In graphic terms, this relationship states that every object point generates a point spread function of the form $1/r$, the center of which lies exactly at this object point and which must still be multiplied by the attenuation coefficient of the object at this position, that is weighted. Experience has shown that approximation images obtained by this simple principle are of practically no diagnostic value [4.26]. Neither fine structures nor small contrast differences can be identified in them. Nevertheless, if the blurring mechanism (described by the $1/r$ function) is known, they contain all the information on the irradiated slice!

Briefly stated, the convolution method attempts to reverse the known blurring process. We recall the generation of the image of an object point in the form $1/r$. This was produced by the superposition of all straight lines associated with the isolated object point, each line having a constant μ value. For a real object, when all the data of a projection are back-projected, the resulting image $\tilde{\mu}_1$ has the appearance of Fig. 4.19. In order to arrive at the approximation image, $\tilde{\mu}$, all these single-projection images have to be superimposed according to the projection direction. However, by modifying all back-projected values along the straight lines in such a way that a negative accompanying component

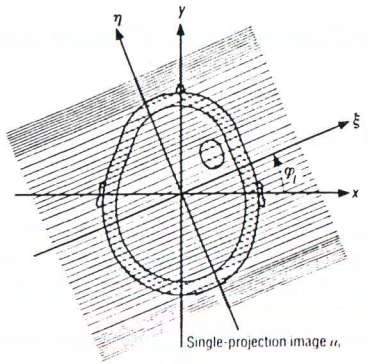

Fig. 4.19
Illustration of the single-projection image corresponding to projection 1

results to the right and left of every straight line as indicated in Fig. 4.20, top right, it is then possible to eliminate the $1/r$ blurring. The positive contributions still acting at any arbitrary distance from the object point along the straight line through the object point are then exactly compensated by the negative contributions of the projections directed oppositely to the projection in question. In the general case of a continuous object, this would be expressed mathematically as the convolution of the projections $p_\varphi(\eta)$ with the function shown in Fig. 4.32 (see page 136) (convolution kernel) and subsequent back projection of the convolution result to the storage device in the radiation direction.

This procedure will be explained using a simplified example (refer to appendix 4.2.3 for a more rigorous mathematical treatment). Fig. 4.20 gives a rough approximation of the convolution kernel by a simpler kernel which assumes only the values 1, $-1/2$ and 0. The three zones in which this kernel is not 0 each have the width of the x-ray scan beam. If two such single-projection images from mutually perpendicular directions are superimposed (Figs. 4.20a and b), a peak of height 2 is produced at the center; it is the "image" of the object point. However, two crossed bars of height 1 extend outwards from this peak to infinity. These bars again have two negative accompanying compo-

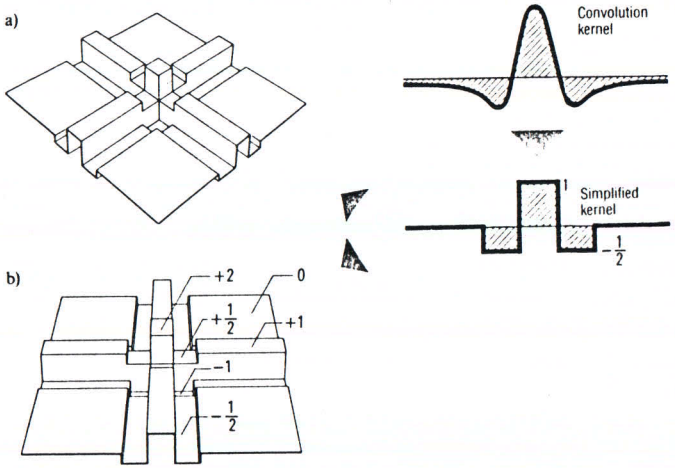

Fig. 4.20
Greatly simplified point image in the convolution method.
With a simplified convolution kernel (right), two crossed projections (left) already produce the "object point" approximately

nents with depth $-1/2$. The negative components are superimposed up to a depth -1 at their intersection points. However, the bars themselves are already partly compensated in the immediate vicinity of the "image point" by the negative components.

In practice, however, not just two crossed projections are used, but several hundred, which are turned to each other at small angular intervals $\Delta\varphi$. We imagine that we first superimpose a further pair of mutually perpendicular projections rotated by 45° (Fig. 4.20a). The result of this superposition is easy to visualize: at the center, the superposition of the four projections yields a peak of height 4. The height of the interfering bars is not increased by this, nor is the depth of their negative accompanying components. The signal-to-noise ratio is therefore improved. In addition, it can be seen that the immediate vicinity of the "image point" is made even more flat. The "holes" of depth -1 which were originally present have been partly filled by the incoming bars. If further such crossed projections are chosen, it can be seen that the central peak will become higher and higher. At the same time, a zone will extend around this peak whose μ values lie close to 0. The positive bars are exactly compensated by the negative accompanying components of neighboring projections.

However, it can also be seen that only a few projections are needed in order to obtain adequate sharpness in the reconstructed image. With an increasing number of projections, the central peak only becomes rounder but no longer narrower. At the same time, though, the ratio of the height of the central peak to the height or depth of the interference streaks becomes larger. The signal-to-noise ratio improves, i.e. the contrast resolution increases (Fig. 4.27 illustrates the effect of choosing too small a number of projections on the reconstructed CT image). On the other hand, the image sharpness is determined by the width of the bars and these in turn by the width of the scanning beam, i.e. primarily by the width of the detector or tube focus.

Critique of the various reconstruction principles

As already mentioned, the algebraic methods are hardly in use any more today. There are two main reasons for this: firstly, the image calculation is only possible after the acquisition of all scan data, so that the doctor has to wait for a longer time; secondly, the computing time is considerably longer than with the convolution method. However, since reconstruction methods are finding increasing application in such clinical areas as nuclear medicine and also ultrasound diagnostics, where the mathematical conditions for the convolution method are only satisfied inadequately, the flexible and versatile iteration techniques may well regain importance.

On the other hand, with the convolution method, every projection is immediately processed in the computer after its measurement, so that there is no waiting

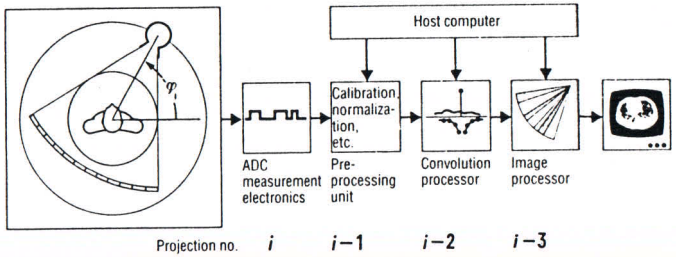

Fig. 4.21 Pipeline principle for reconstructing a CT image in real time

time for the doctor between the completion of the measurement and the appearance of the image on the screen.

In principle, all the above-mentioned considerations can be applied to the fan-beam system. However, the computer time required for image reconstruction increases unavoidably.

In order to reconstruct a CT image in real time, i.e. while the measurement data is being transferred to the computer, the so-called pipeline principle is used (Fig. 4.21). While projection No. i is undergoing analog-digital conversion and is being transferred to the computer, the immediately preceding measured projection is already undergoing the necessary preprocessing steps; its predecessor is convolved at the same time and its predecessor in turn already being back-projected. Of course, the processing speed for this operating principle is determined by the most critical time element in the chain, i.e. by the back projection. Therefore, special computers must be used, which have been especially designed for executing this operation. On the other hand, the pipeline principle cannot be applied to ring-detector systems with a stationary detector array. With this type of machine, we must first collect and rearrange all the measured values registered by a detector during the rotation of the tube before the convolution can take place.

Remarks on image reconstruction algorithms for the fan-beam principle

According to Jass [4.27], the convolution relationship (4.22) can be directly adapted to the fan-beam principle (Fig. 4.22). For this, the linear coordinate η must be replaced by the angular coordinate ψ and the filtering carried out using the function $\cos\psi\, p_\varphi(\psi)$. The position P at which the convolution product should be plotted must, however, already be included in the calculation of the convolution product; the distance from the image point P in question to

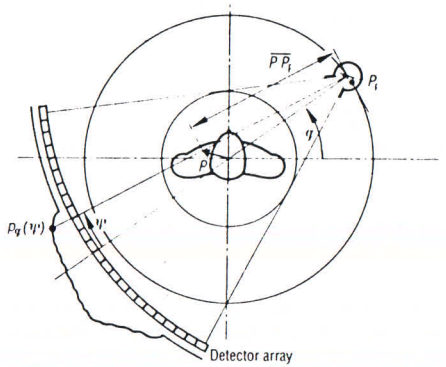

Fig. 4.22
Coordinate system of a fan-beam machine

φ Projection angle
ψ Angle within the fan
P Image point to be reconstructed
P_f Momentary focal spot
P_φ Projection

the momentary projection center P_f appears in the convolution integral. Under certain conditions, however, this distance can be eliminated from the convolution integral, so that the computational requirements are drastically reduced and resemble more the computational requirements of the convolution method for the parallel-beam scanner. This means that data processing can keep in step for fan-beam systems, with all the advantages for practical clinical operation. The Somatom fan-beam scanner, equipped with a special processor, functions according to this principle.

4.2.2 Image quality

The following are the principal criteria used for evaluating image quality in CT:

spatial resolution
contrast resolution (differentiation of fine differences in tissue density),
absence of all types of artifacts.

Apart from these, the following factors are of key importance in determining the image quality which can be attained in practice:

scan time and
required dose per image slice.

Since it seems hopeless to attempt to deal with all aspects of this comprehensive area, even in an approximate fashion, only characteristic differences between the CT image and the classical x-ray image will be indicated here.

Essentially, these differences arise from two sources. Firstly, the physical measurement process does not immediately yield the CT image. This can only be reconstructed with the help of the above-described mathematical transformation from all the measured data. The computing process destroys the local character of the measurement errors, unavoidable as in any measurement procedure, and distributes them over the entire image in a manner which is typical for the type of measurement error. The location at which an image distortion originates and the location of the distortion in the image are therefore no longer necessarily identical.

The second difference compared to classical radiography is discretization, i.e. the determination of the attenuation capacity of the tissue by only a finite number of measurement data. Only if certain rules are obeyed, of which the well-known Shannon sampling theorem [4.28] is the most important, is this procedure justified. The non-observance of these rules also produces image distortions unknown to classical radiography.

If we wish to understand the implications of the fact that the CT image is a computer-generated image derived from a few hundred thousand measured data, then we must keep in mind the two most important image reconstruction procedures. These are:

convolution, by means of which every projection is transformed so that negative projection values are also obtained, and
back projection, which imposes the convolved scan data in the direction of the scan beam onto the recording medium.

The different reaction of different scanner types to measured value disturbances

It is immediately understandable that disturbances in individual sample values of a single projection result in different image disturbances than uniform distortions of the measured data of a projection or even of all projections. This means that different CT scanning principles react to the same measured value disturbances with different image disturbances. For example, in a fan-beam scanner with a rotating detector array (see Fig. 4.7d), all data from a single projection are distorted in the same way as a result of fluctuations in the tube voltage, but different projections are distorted differently, whereas with a ring-detector scanner (see Fig. 4.7c) with stationary detectors, in which the data from one projection are collected during the movement of the x-ray tube, fluctuations in the measured data result in fluctuations within the projections. The following artifact examples relate to fan-beam scanners.

Typical CT image disturbances

The best way to understand image disturbances in computed tomography is to simulate their sources in a computer model. Synthetic scan data are generated which are distorted in a defined manner. In this way all other sources for measurement distortion, which are always present in reality, are eliminated. As in any measurement procedure, in computed tomography one has to distinguish between systematic and statistical measurement errors.

Systematic measurement errors

Distortion of a single measurement value

Let us consider the extreme case that one out of approximately 2×10^5 to 10^6 measured values is lost. This measured value disturbance is now also subjected to the convolution process for the affected projection, in the course of which accompanying components with opposite sign are produced to the right and left. The back projection thus generates a 3-line structure corresponding to Fig. 4.20, as shown in Fig. 4.23a.

Uniform distortion of a projection

We will again consider the extreme case in which an entire projection drops out. In this case, we do not have the reinforcing effect of the convolution operation on the distortion. We obtain the dark bars ascribed to objects of high density, as can be seen in Fig. 4.23b. It becomes clear that a serious disturbance in the measured data, namely the absence of an entire projection, which in this case involves 256 measurement values, results in a less pronounced image distortion than if a single measurement value drops out. In general, the following rule of thumb applies: disturbances in a single measured value within a projection are easier to recognize in the CT image than those which affect an entire projection in the same manner.

Statistical fluctuation phenomena

Here, we must first mention the so-called quantum noise, i.e. a physically unavoidable statistical fluctuation of the x-ray beam intensity, the effects of which can only be reduced by increasing the x-ray dose. In addition, however, statistical fluctuations are also involved to a certain extent in the electronics and the scanning mechanism.

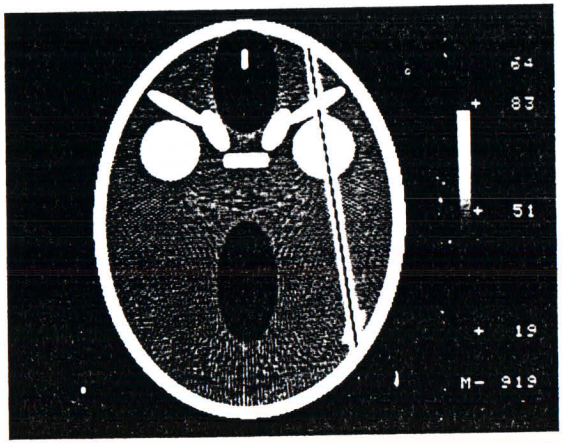

a) 3-line structure (white/black/white) when a single measured value is missing

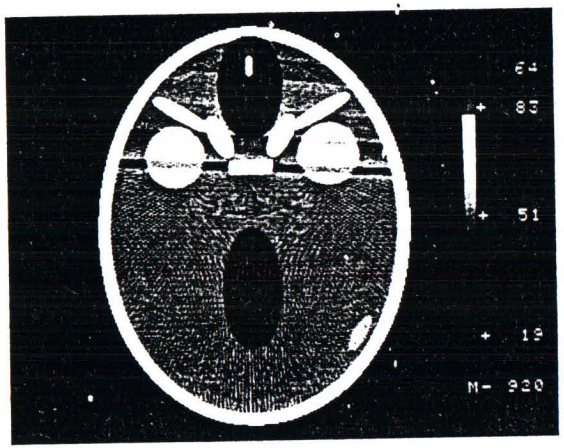

b) Interference structure when an entire projection is missing

Fig. 4.23
The simulated skull phantom shows a high-contrast structure ("bones", i.e. white), for example the "skull" and an "air inclusion" (black), as well as low-contrast structures, for example the "ventricle" and a small "hematoma" below the center of the image

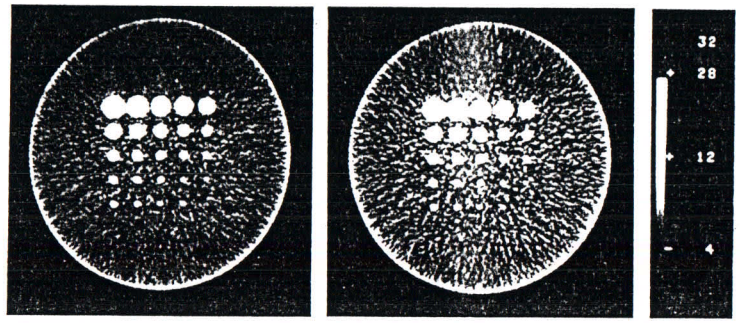

80 mGy 40 mGy

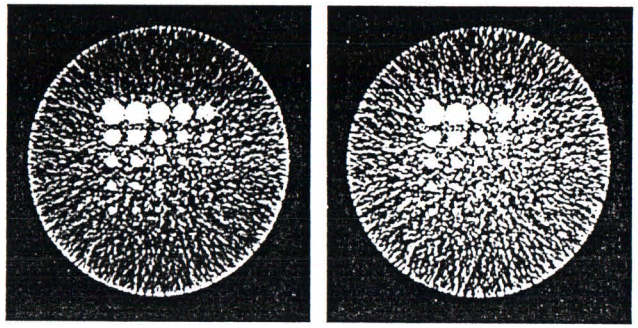

10 mGy 2,5 mGy

Fig. 4.24
"Button card": rods in the water bath. The density of the rods decreases from left to right. The preferential radial direction of the noise islands at the edge of the object should be noted. The dose per slice image is given in milliGrays (mGy)

Fig. 4.24 shows the so-called "button card", a simulated, water-equivalent plate, in which rods of variable diameter and variable density are embedded. The density decreases from left to right. With a decreasing x-ray dose per slice image, the noise disturbances are superimposed onto the object structures and make it difficult to identify them. A radial preferential direction of the noise islands to the edge of the object can be observed as an important characteristic of the CT image.

Basic remarks on the perceptibility of artifacts

It can be expected that statistical disturbances also make the recognition of systematic measurement errors more difficult. However, more exact investigations show that measurement errors associated with noise must reach an unacceptable level in many cases before they effectively mask systematic errors. Thus, in the case shown in Fig. 4.25, the fluctuation of the image noise is about the same as for the marked band or ring distortion structures immediately recognizable by the eye. The large "ventricle" below the center of the image differs from its environment by only half the noise fluctuation, σ, and the same applies to the "hematoma" which can still be recognized in the bottom right of the image.

Obviously, our visual perception system plays an important part in recognizing artifacts. The eye seems to look over the image for large simple structures and in this manner smooths over local statistical fluctuations in brightness.

Matching of the system parameters

The resolution capacity of a CT system is primarily determined by the scan beam width, i.e. by the effective widths of the focus and detector. If the beam width is predefined, the distances between the detectors, the angles between

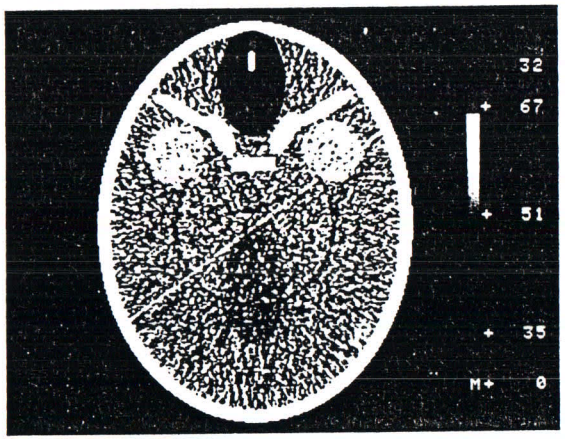

Fig. 4.25
Difference in the recognizability of systematic and statistical image distortions. Extended, coherent structures (band, ring, "ventricle", "hematoma") can be easily identified in spite of the noise

neighboring projection directions, the height of the slice to be measured and finally the fineness of the image matrix must be correctly matched to each other. The correct choice of these parameters is a complex optimization problem, which must take special account of the discrete nature of the data acquisition.

In order to be able to calculate an image from the measured data which is as true as possible to the object, it is necessary to fill up the measurement plane in all directions with measurement lines. Strictly speaking, this is not possible with a finite number of measurement lines. Fortunately, however, as was already emphasized earlier, the scan beam has a finite width, so that instead of the line integrals only integrals averaged over the finite-width measurement bands can be obtained. These can be approximately regarded as line integrals over an averaged, i.e. blurred, object function. The measurement system therefore produces a low-pass filtering of the object and thus suppresses fine structures. It is plausible that the remaining smoothed structures can be fully processed by scanning in finite steps, which is in fact essentially the statement of the Shannon sampling theorem [4.28]. Applied to functions of one variable (e.g. time), this states:

If point-like "samples" are taken from a frequency-band limited, i.e. low-pass filtered, function $g(t)$ at regular intervals ΔT, then the original function can be completely reconstructed from these "samples" alone, as long as the interval ΔT between neighboring samples is chosen sufficiently small. ΔT must be chosen so that at least two "samples" are still taken in each period from the highest frequency structures still contained in the function to be scanned.

The required number of projections and measured data per projection can be derived from this requirement for a given scanning beam width for every CT system. For example, for a parallel-beam machine in which the focus only traverses an angle of 180°, it can be estimated that the number of projections should be approximately $\pi/2$ times the number of measured values within a projection.

However, the situation is not so clear for fan-beam and ring-detector systems. During the scanning process, it can happen that – due to an exchange of roles between the focus and detector – scan beams are duplicated. The measured data are therefore not necessarily independent; their number is consequently not a direct measure for the fineness of scanning. This coincidence of the measurement beams can be avoided by mounting the detector array in a well defined position, slightly unsymmetrically to the center line of the focus-rotation center [4.29]. Fig. 4.26 shows the effectiveness of this simple trick.

Of course the requirement for a sufficiently fine scanning of the approximately band-limited projections must be balanced against the requirement for a sufficient number of projections. Nevertheless, since the sampling theorem states that, for restricted bands, increasing the number of projections above a certain limit does not bring any further benefit, it is part of the designer's job to exactly meet those hardware requirements which are necessary and at the same time

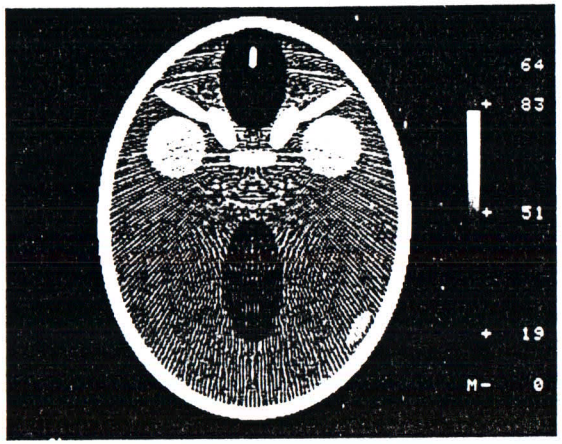

a) Centered detector array

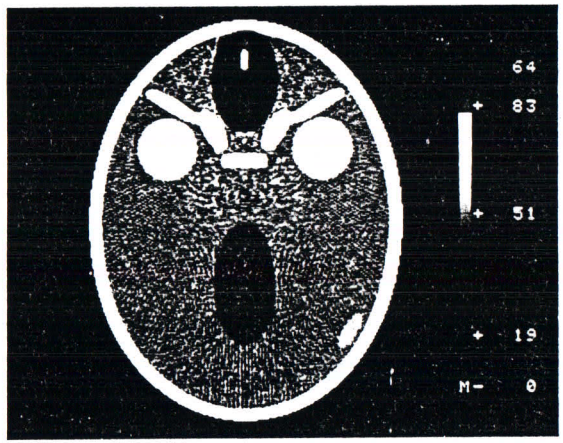

b) quarter shift offset of the detector array

Fig. 4.26
Reduction of artifacts by quarter shift offset of the detector array

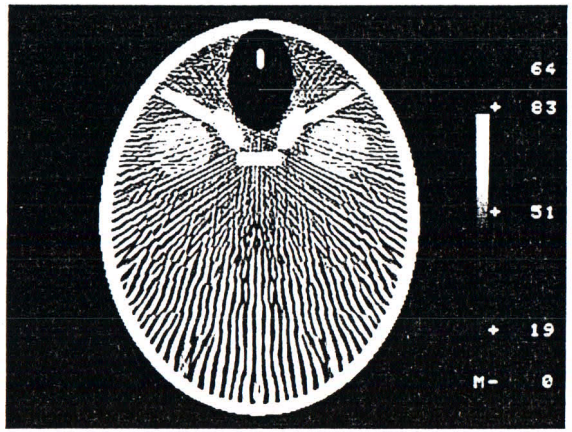

a) 180 projections

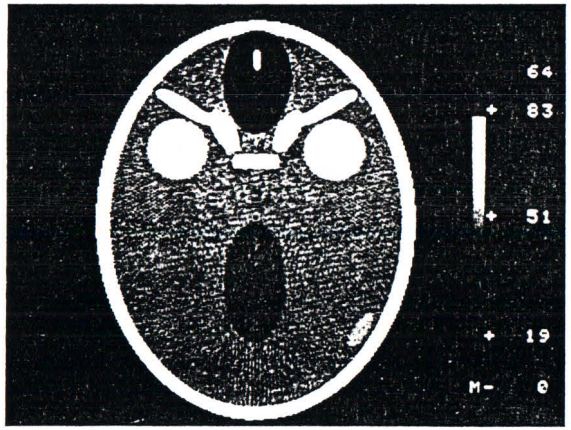

b) 720 projections

Fig. 4.27
Matching the number of projections to the scan beam width

just sufficient. Fig. 4.27a shows the case of faulty matching of the number of projections to the scanning beam width. For an effective scan beam width of approximately 1.5 mm, 180 projections are obviously still not sufficient, while according to Fig. 4.27b 720 projections are already clearly sufficient. The easily recognizable dark "ventricle" (fine contrast −5‰) in the bottom third of the image could not be made visible with 180 projections, just as with the clearly recognizable "hematoma" (fine contrast +5‰) with 720 projections at the bottom right. Thus, faulty matching of the number of projections to the scan beam width may make the recognition of large low-contrast structures very difficult.

The last example illustrates the problems of discretization, namely the fact that the CT image is obtained from individual data samples. If, in order to limit the computational requirements, the number of detectors is kept constant, but – in order to increase the spatial resolution – the focus and detectors are chosen to be very narrow, the artifacts of Fig. 4.28 will then result.

Such a measure would consequently not result in the desired improvement in detail sharpness, but in fact generate new image distortions. From classical

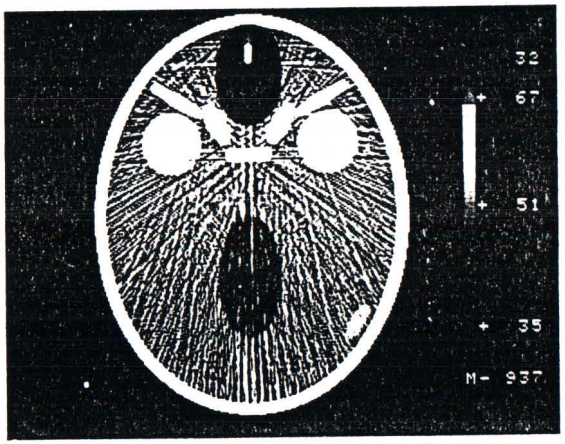

Fig. 4.28
Scanning with an "ideal", infinitely thin scanning beam but a finite number of measured data

radiography there is no parallel to such a phenomenon, arising specifically from the discretization of data. In radiography, one would expect that if the focus and detector are made smaller (for the latter we can consider using a film with sharper definition), an increase in spatial resolution without extensive distortion should result.

Discussion of a few frequently observed CT artifacts

Table 4.1 classifies the possible noise sources, dividing them into different groups with typical examples of each.

From the group of physically induced measurement errors, we consider here the beam hardening effect (see Sect. 4.1.6) and the non-linear partial volume effect, which nearly always occur together in an actual CT image and can therefore hardly be separated.

As already mentioned, an x-ray tube emits radiation of varying energy. However, since biological tissue absorbs soft x-rays more strongly than hard x-rays, when the scan beam penetrates the center of the body the x-rays emerging are harder than when the beam penetrates the body peripherally.

Table 4.1 Causes of CT artifacts

Physical causes
• Quantum noise
• x-ray scattering by the patient
• Beam hardening
• Non-linear partial volume effect
Patient-related effects
• Movement of the patient or of individual organs
• Overcharge of the data acquisition system due to metallic foreign objects
System-related causes
• Design insufficiencies
Faulty matching of scan parameters
Inadequacies in the image reconstruction algorithm
• System faults, such as
Non-uniform scanning movement
Fluctuations in the x-ray tube voltage
Temperature drift in the measurement electronics

In the first case, this means that the detector sees a smaller attenuation capacity for the tissue. Modern CT systems are generally able to correct for this systematic error, in most cases adequately for diagnostic purposes.

However, this correction is based on the assumption, which is not strictly correct, that only varying tissue density is responsible for the differences in attenuation capacity of the tissue and not differences in atomic composition. Therefore, when bones are irradiated there are always residual errors which, for example, appear as dark bars between the petrous bones in cranial scans.

On the other hand, the non-linear partial volume effect arises as a consequence of the exponential, i.e. non-linear, attenuation of the radiation when high-contrast structures are only partially immersed in the slice to be imaged. This effect therefore always accompanies the beam hardening effect with bones. Rührnschopf and Kalender [4.30] succeeded in discovering the main differences between these effects by the skillful use of linear and non-linear combinations of the measured data from neighboring slices (Fig. 4.29). This eliminated soft-tissue structures which would hamper the interpretation. In this way, it was possible to show that the non-linear partial volume effect was the cause of the star-shaped artifact emerging from the protuberantia occipitalis in the fossa posterior. In principle, it is possible to largely eliminate the beam hardening effect with the help of intermittent spectral measurements [4.19], but the price for this is a considerable increase in expenditure.

On the other hand, correction methods based on the estimated bone distribution derived from the normal monospectral CT image have not gained acceptance,

a) b)

Fig. 4.29
Isolated display of the non-linear partial volume effect (a) and the radiation hardening effect (b)

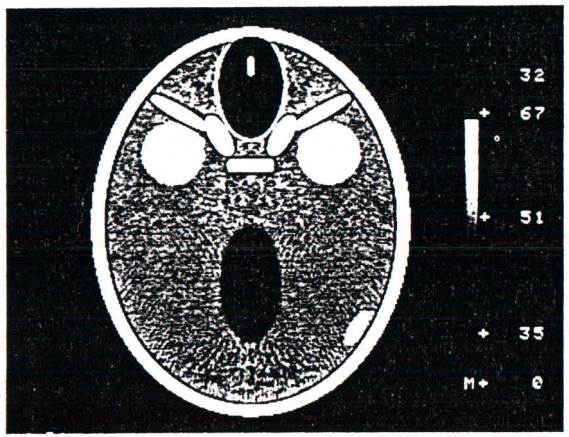

Fig. 4.30
Simulation of a high detail sharpness by modification of the convolution in order to emphasize the edges. The apparent "subarachnoidal space" should be noted

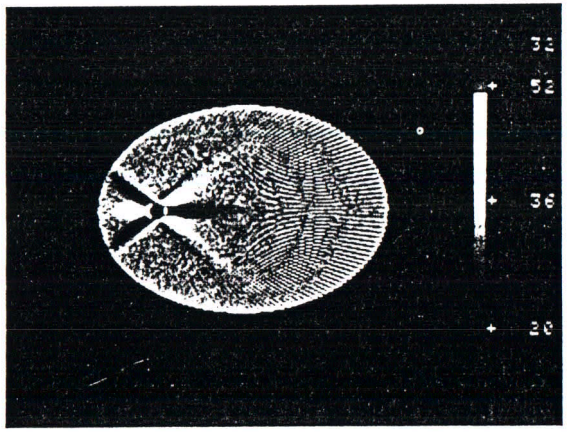

Fig. 4.31
Interference structure in the form of a cross produced by moving an "intestine" filled with contrast medium during the scan

one reason being that they require a very exact specification of the calcium content of the bone.

The non-linear partial volume effect can only be reduced by using thinner slices.

Fig. 4.30 shows an example from the group of system-related measurement errors. Here, the convolution method was modified in order to ensure edge enhancement, such as at the borders between bones and soft tissue. Many manufacturers provide the user with such means for specific alteration of the image character. Despite their undisputable usefulness in terms of diagnosis, the risk of an incorrect interpretation must be pointed out: the "subarachnoidal space" apparently shown in Fig. 4.30 is a pure artifact (compare with Fig. 4.27b).

As an example of a patient-related image distortion we show a motion artifact caused by peristalsis. If an "intestinal balloon" wetted with contrast agent is moved somewhat from its resting position during the scan time and then moved back, the image shows a typical distortion structure in the form of a cross (Fig. 4.31). Although such a structure is relatively easily recognized as a motion artifact in the CT image, the combination of several such artifacts can make it considerably more difficult to interpret the image.

4.2.3 Mathematical appendix: description of the convolution method

Filter equation

Equation (4.8) assigns a function $p_\varphi(\eta)$ of the variables φ and η to the distribution of the attenuation coefficients μ in the intersection plane. This function is called the Radon transform of μ. Already in 1917, Radon developed an integral transformation for recovering the function μ from the projections $p_\varphi(\eta)$ [4.21]. The relationships between the Radon transformation and the Fourier transformation [4.31] make it possible to represent the Radon inverse transformation in terms of the generally more commonly used Fourier transformation.

If one neglects higher-order physically caused effects, the CT measurement process represents a linear, position-invariant system in which the point spread function is derived as $1/r$. A real distribution of μ values provides the superposition of all point images weighted according to this distribution, i.e. the convolution product

$$\bar{\mu}(\underline{r}) = \iint \mu(\underline{r}') \frac{\gamma}{|\underline{r} - \underline{r}'|} \, \mathrm{d}^2 \underline{r}'. \tag{4.11}$$

This can be written in the more compact form

$$\bar{\mu} = \mu^* \frac{\gamma}{r}, \tag{4.12}$$

where $\gamma = 1/\text{cm}$ is a constant which ensures that the physical dimensions are the same on both sides of the equation (4.12).

In order to obtain the distribution $\mu(r)$ from this relationship, we first make use of the two-dimensional Fourier transform $F_2\{\bar{\mu}\}$ and obtain, with the help of the convolution theorem,

$$F_2\{\bar{\mu}\}(\underline{v}) = F_2\{\mu\}(\underline{v}) \cdot \frac{\gamma}{v}, \tag{4.13}$$

with

$$F_2\left\{\frac{1}{r}\right\} = \frac{1}{v} \quad \text{and} \quad v = |\underline{v}|.$$

$\underline{v}$ denotes the two-dimensional frequency vector (see Sect. 2.2 for the meaning of the frequency vector).

We now obtain the required solution of equation (4.8) from equation (4.13), the so-called filter equation

$$\mu(\underline{r}) = \frac{1}{\gamma} F_2^{-1}\{v F_2\{\bar{\mu}\}\}(\underline{r}),$$

which, however, is best generalized to

$$\mu^*(\underline{r}) = \frac{1}{\gamma} F_2^{-1}\{H(v)\, F_2\{\bar{\mu}\}\}(\underline{r}). \tag{4.14}$$

Here, $H(v)$ represents a suitable filter function. If, for example, one knows that the measured spatial frequency spectrum has already fallen off to zero above a frequency limit v_0, $H(v)$ can be arbitrarily chosen for $v \geq v_0$.

The filter equation (4.14) provides the possibility for influencing the nature of the image in a controlled manner by a suitable choice of $H(v)$. For example, by raising the filter function for high spatial frequencies, the contour sharpness can be enhanced or images with low noise can be obtained with the help of suitable band-pass filters.

Nevertheless, one of the disadvantages of an image reconstruction algorithm based on equation (4.14) would be that at best the superposition image $\bar{\mu}$ could be reconstructed in the computer during the scan process, but the filtering could only be carried out after completion of the scan. Concurrent data processing would therefore be impossible.

One-dimensional form of the filter equation

We will show below how to simplify the filter equation to make it suitable as a basis for the real-time processing of scan data.

Let the unit vector which points in the direction of the linear scanning movement be denoted by $\underline{t}_\varphi$ (see Fig. 4.15). The unit vector $\underline{s}_\varphi$ perpendicular to it points in the direction of the scan beam. Then, the approximation image $\bar{\mu}$ introduced in equation (4.12) can be expressed in terms of the projections p_φ:

$$\bar{\mu}(\underline{r}) = \gamma \int_0^\pi p_\varphi(\underline{r} \cdot \underline{t}_\varphi)\, \mathrm{d}\varphi. \tag{4.15}$$

Equations (4.14) and (4.15) represent the relationship between the projections and the distribution μ. It can be shown that equation (4.15) also yields the point spread function γ/r.

Since the function $\gamma p_\varphi(\underline{r} \cdot \underline{t}_\varphi)$ only varies along one direction, namely along the scanning direction $\underline{t}_\varphi$, but not along the direction of the beam $\underline{s}_\varphi$, it can be regarded as a stripe image.

If we now wish to transform the filter equation with the help of equation (4.15) so that the superposition is only performed after the filtering, then we first calculate the Fourier integrals

$$F_2\{p_\varphi(\underline{r} \cdot \underline{t}_\varphi)\}(\underline{v}) = \iint p_\varphi(\underline{r} \cdot \underline{t}_\varphi)\, \mathrm{e}^{-j2\pi \underline{r} \cdot \underline{v}}\, \mathrm{d}^2\underline{r},$$

by introducing the coordinate transformation

$$\xi = \underline{r} \cdot \underline{s}_\varphi, \quad \eta = \underline{r} \cdot \underline{t}_\varphi, \quad u = \underline{v} \cdot \underline{s}_\varphi, \quad v = \underline{v} \cdot \underline{t}_\varphi \tag{4.16}$$

Since $\underline{r} \cdot \underline{v} = \xi u + \eta v$ and $\mathrm{d}^2\underline{r} = \mathrm{d}\xi\, \mathrm{d}\eta$, we obtain

$$\begin{aligned} F_2\{p_\varphi(\underline{r} \cdot \underline{t}_\varphi)\}(\underline{v}) &= \int_{-\infty}^{+\infty} p_\varphi(\eta)\, \mathrm{e}^{-j2\pi\eta v}\, \mathrm{d}\eta \int_{-\infty}^{+\infty} \mathrm{e}^{-j2\pi\xi u}\, \mathrm{d}\xi \\ &= F_1\{p_\varphi\}(v) \cdot \delta(u). \end{aligned} \tag{4.17}$$

Here $\delta(u)$ is the well-known Dirac function.

The two-dimensional spectrum of a stripe image $\gamma p_\varphi(\underline{r} \cdot \underline{t}_\varphi)$ is therefore concentrated on a straight line in the frequency plane. This line runs parallel to the scanning direction. If we now substitute equation (4.15) into the filter equation (4.16), taking into consideration equation (4.17), then after exchanging the order

of integration and setting $v^2 = u^2 + v^2$, we obtain

$$\mu^*(\underline{r}) = \int_0^{\pi} F_2^{-1}\{H(v)\, F_2\{p_\varphi(\underline{r}\cdot\underline{t}_\varphi)\}\}\,\mathrm{d}\varphi$$

$$= \int_0^{\pi}\int_0^{r} H(|r|)\, F_1\{p_\varphi\}(r)\, \mathrm{e}^{j2\pi\eta r}\,\mathrm{d}r\,\mathrm{d}\varphi$$

$$= \int_0^{\pi} F_1^{-1}\{H(|r|)\, F_1\{p_\varphi\}(r)\}\,\mathrm{d}\varphi. \qquad (4.18)$$

This relationship represents a version of the filter equation (4.14) which allows concurrent image reconstruction, because it now contains only computational operations which can be executed with the individual projections p_φ. Every projection can be filtered immediately after its measurement and back-projected. However, the filtering can also be performed directly on the measured values without having to proceed via the Fourier space. If we choose the one-dimensional convolution kernel $h(\eta)$ so that

$$H(|r|) = F_1\{h\}(r) \qquad (4.19)$$

the convolution theorem along with equation (4.11) yields

$$\mu^*(\underline{r}) = \int_0^{\pi} (h * p_\varphi)(\underline{r}\cdot\underline{t}_\varphi)\,\mathrm{d}\varphi$$

$$= \int_0^{\pi}\left(\int_{-r}^{+r} h(\underline{r}\cdot\underline{t}_\varphi - \eta)\, p_\varphi(\eta)\,\mathrm{d}\eta\right)\mathrm{d}\varphi. \qquad (4.20)$$

$\mu^*(\underline{r})$ now represents a superposition of one-dimensional convolution results.

Discretization of the filter equation

For digital data processing, φ can only assume M different, normally equidistant, positions φ_m:

$$\varphi_m = m\Delta\varphi \quad \text{with } \Delta\varphi = \frac{\pi}{M} \quad \text{and} \quad 1 \le m \le M.$$

The projections, too, are only known at N equidistant points $\eta_n = na$, where the measured projection values only represent approximation values for $p_\varphi(\eta_n)$, denoted by $p_{\varphi,n}$; a is the sampling interval.

These approximation values must now either be filtered after discretization of equation (4.18), which can be facilitated by the fast Fourier transformation (FFT), or discretely convolved using equation (4.20) with a suitable numerical sequence h_k. If we consider the values $\bar{p}_{\varphi,n}$ as the scanning values of a continuous function $\bar{p}_\varphi(\eta)$, the question arises under what conditions the actual convolution integral to be calculated

$$g(\eta) = \int_{-\infty}^{+\infty} \bar{p}_\varphi(\eta')\, h(\eta-\eta')\,\mathrm{d}\eta' \qquad (4.21)$$

may be replaced by discrete convolution expressions of the form

$$g_k = a \sum_{n=-\infty}^{+\infty} \bar{p}_{\varphi,n}\cdot h_{k-n} \qquad (4.22)$$

(For formal reasons, the summation and integration limits are assumed to be infinite).

There is a simple answer to this question. If we assume that the functions $\bar{p}_\varphi(\eta)$ and $h(\eta)$ are frequency-band limited with a bandwidth $B \le 1/(2a)$, then the following relationship applies exactly

$$a \sum_{n=-\infty}^{+\infty} \bar{p}_{\varphi,n}\cdot h_{k-n} = \int_{-\infty}^{+\infty} \bar{p}_\varphi(\eta')\cdot h(ak-\eta')\,\mathrm{d}\eta', \qquad (4.23)$$

if the h_k are chosen as sampling values $h_k = h(ak)$ of the continuous kernel $h(\eta)$. This follows immediately from the representation which is valid for any functions $f(\eta)$ of bandwidth B:

$$f(\eta) = \sum_{k=-\infty}^{+\infty} f\left(\frac{k}{2B}\right)\cdot S_k(\eta), \qquad (4.24)$$

where $S_k(\eta)$ is an abbreviated notation for

$$\frac{\sin 2\pi B(\eta - k/(2B))}{2\pi B(\eta - k/(2B))}$$

and from the easily verified relationship

$$\int_{-\infty}^{+\infty} S_k(\eta')\cdot S_n(\eta-\eta')\,\mathrm{d}\eta' = a\cdot S_{k+n}(\eta). \qquad (4.25)$$

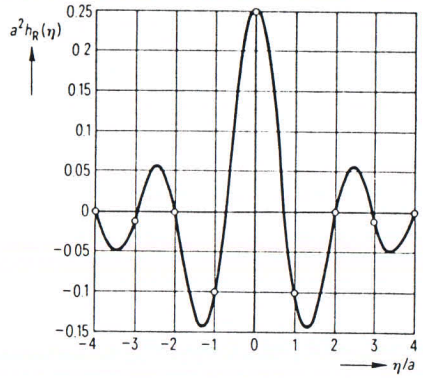

a) Ramachandran-Lakshminarayanan kernel

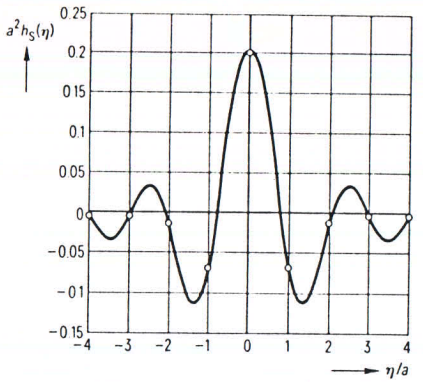

b) Shepp-Logan kernel. Solid lines represent $h(\eta)$ and circles h_k (cf. Table 4.2)

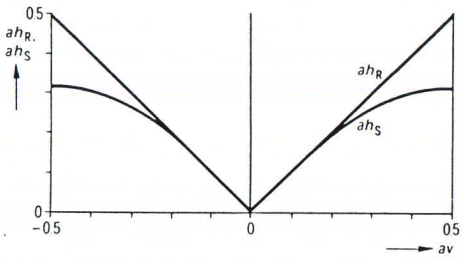

c) Representation of the filter functions corresponding to h_R and h_S

a sampling interval length

Fig. 4.32 Illustration of the two most common convolution kernels

The most common convolution kernels in x-ray computed tomography are the kernel $h_R(\eta)$ of Ramachandran and Lakshminarayanan [4.24] and the kernel $h_S(\eta)$ of Shepp and Logan [4.25].

The former, historically older, represents the implementation of the frequency filtering

$$H_R(v) = |v| \cdot \mathrm{rect}(av) \tag{4.26}$$

and the latter the implementation of the frequency filtering

$$H_S(v) = |v| \cdot \left| \frac{\sin \pi v a}{\pi v a} \right| \cdot \mathrm{rect}(av). \tag{4.27}$$

Here, $\mathrm{rect}(x)$ is the well-known rectangular function, which is 1 for $|x| \leq 1/2$ and 0 for $|x| > 1/2$. These kernels and their Fourier transforms, i.e. their associated frequency filters, are compared in Table 4.2. A graphical representation is shown in Fig. 4.32.

Table 4.2
Equivalent representations of the two most important convolution kernels

	Kernel of	
	Shepp and Logan	Ramachandran and Lakshminarayanan
h_k	$-\frac{2}{\pi^2 a^2} \frac{1}{4k^2-1}$	$\frac{1}{4a^2}$ $k = 0$ 0 k even, $\neq 0$ $-\frac{1}{\pi^2 a^2 k^2}$ k odd
$h(\eta)$	$-\frac{2}{\pi^2 a^2} \frac{1 - 2\frac{\eta}{a}\sin \pi \frac{\eta}{a}}{4\left(\frac{\eta}{a}\right)^2 - 1}$	$\frac{1}{2a^2}\left\{\frac{\sin \pi \frac{\eta}{a}}{\pi \frac{\eta}{a}} + \frac{\cos \pi \frac{\eta}{a} - 1}{\left(\pi \frac{\eta}{a}\right)^2}\right\}$
$H(\lvert v \rvert)$	$\lvert v \rvert \cdot \left\lvert \frac{\sin \pi v a}{\pi v a} \right\rvert \mathrm{rect}(av)$	$\lvert v \rvert \mathrm{rect}(av)$

8 X-ray computed tomography

8.1 Equipment design

There are different types of requirements for a computer tomograph (CT). For example, although the main requirement for a skull image is the best contrast resolution, the exposure time being of minor importance, an image of the torso requires the shortest possible exposure time. Only then can one be certain that organ movements, respiration or peristalsis do not cause any interference in terms of image artifacts.

8.1.1 The CT system and its components

The components of a CT system are shown in the block diagram (Fig. 8.1). The operating console is the central communication unit for the user of the system. All equipment parameters and patient data are input here. The scan itself is initiated from here and here the reconstructed image is displayed on a monitor. A well designed operating concept is characterized by as few input

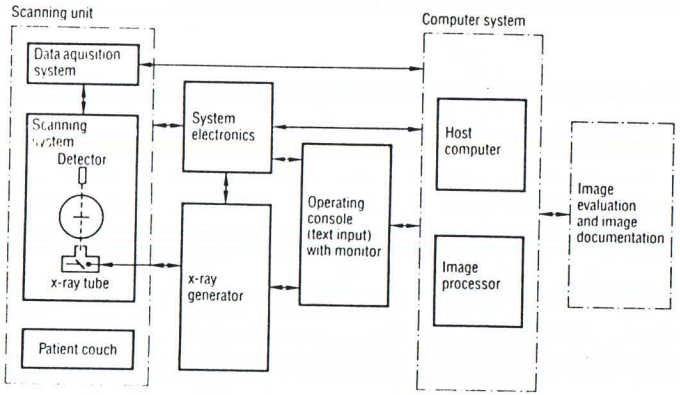

Fig. 8.1
Schematic diagram of a CT scanning system

procedures as possible which are as simple as possible. The computer system provides support to the operator and controls and monitors safety functions. The fastest possible imaging computer for image reconstruction forms the heart of the computer system. The scanning system with x-ray tube, diaphragm and detector as well as the electronics for processing the measurement data and the patient couch form the scanning unit. Here, the scanning system and the data aquisition system are housed in the scanning system, i.e. in the gantry. The x-ray generator, characterized by high output power and constancy of its output values, and also the system electronics are essential components of a CT system which, as the components for image evaluation and image documentation, are controlled by the computer system.

8.1.2 Scanning unit

Fig. 8.2 shows the scanning unit of a whole-body CT. The gantry can be tilted by $+/-25°$; the patient is moved into the measurement field on a couch. Seen from the outside, it is impossible to tell what is the operating principle of a CT scanner. The magnitude of the measurement field, the diameter of the measurement aperture and their accessibility from all sides determine the possible field of application.

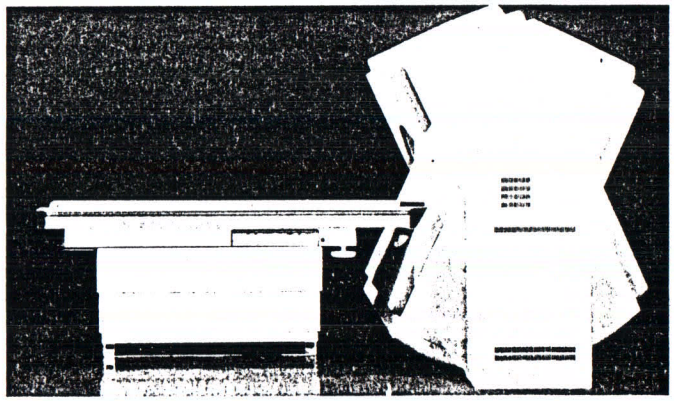

Fig. 8.2
The tilting gantry of a whole-body computer tomograph facilitates the measurement of coronary sections and allows the free projection of organs

8.1.2.1 Gantry

A parallel beam apparatus based on the translation-rotation principle requires alternating linear and rotational movements of the detector system, which is rigidly connected to the x-ray tube. It is understandable that, because of the relatively large mass, the exposure times have lower limits imposed on them. At present, measuring times as low as approximately 10 seconds can be achieved.

However, the most commonly used apparatus functions according to the fan-beam principle. Here, a distinction is made between scanning systems with detector and x-ray tube rotating with them and those with rotating x-ray tube and stationary detector ring. In installations with rotating x-ray tube-detector systems, several hundred radiation receivers are arranged on a circular arc opposite the x-ray tube with the focal spot as the center (Fig. 8.3). The large number of detector elements and scanning channels process a corresponding number of measured signals at the same time. This means that the scanning procedure is reduced to a single rotation movement, which allows short exposure times of less than one second for large scanning field diameters of, for example, 50 cm. Monitor detectors at the edge of the diaphragm system next to the x-ray tube constantly measure the unattenuated x-ray radiation outside the patient scanning field for normalization purposes. The x-ray tube is operated with constant radiation or in pulse mode. The demands made by the large number of scanning channels means that only the scanning of one slice per exposure is economically viable.

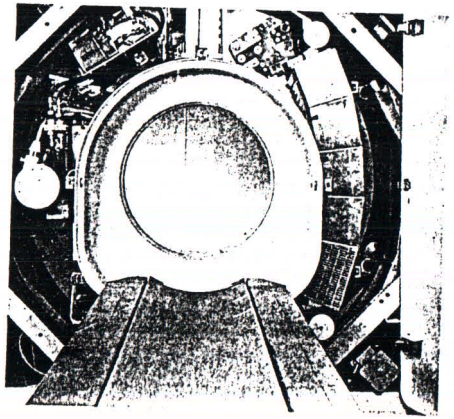

Fig. 8.3
Gantry unit
of the SOMATOM DR
fan-beam scanner,
with rotating detectors

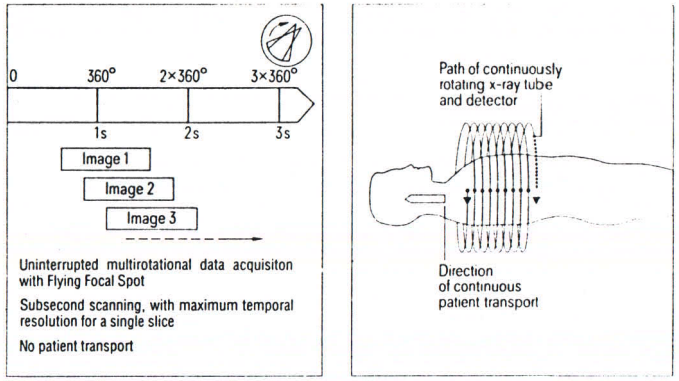

Fig. 8.4
Dynamic Multiscan with and without patient transport (Somatom Plus)

Very high demands are placed on the mechanical components. In these systems, the position of the "projection" must be known to a fraction of a degree and the positioning of the detector elements must be known to 0.01 mm. The short exposure times and interscan times enable a slice frequency of more than 10 slices per minute and thus make it possible to operate in "CT-angio" mode.

The latest generation of high-performance CT systems (SOMATOM PLUS) operates with continuous rotation of the radiation detector system and flying focal spot. This allows measurement times of less than 1 second and successive exposures without any breaks (Fig. 8.4). The continuous moving of the patient transport during this procedure allows the scan of a continuous volume of the body.

8.1.2.2 Patient positioning and slice positioning

The patient couches of these CT systems have adjustable height and can be adjusted to the height of the bed when it is necessary to transfer the patient. The patient on the couch is raised to the operating height and then moved into the exposure position. Tilting visors, a tilting gantry and automatic advance of the couch make it possible to provide a rapid and reproducible slice positioning. Fig. 8.5 shows an example of this.

The functions necessary for positioning the patient can be directly controlled from the couch, the gantry or remotely controlled from the central operating console.

In addition, locating the correct slice can be considerably facilitated by means of a localizer radiograph (Topogram) (Fig. 8.6). With this imaging principle, the scanning system remains in a fixed position, e.g. x-ray tube above and detectors underneath the patient. The patient is then moved through the measurement aperture. The "line profiles" obtained in this way are combined by the computer to form an image and displayed on the monitor. The image produced in this way corresponds to a parallel projection in the forward movement direction of the patient and a central projection in the direction perpendicular to this. The dose applied for such an exposure is very low. The high density resolution and the possibility of displaying a good contrast area facilitate the slice definition. With the help of superimposed marks, the patient is automatically moved to the required exposure position (Figs. 8.7 and 8.8). This imaging mode can also be directly used for producing a diagnosis.

8.1.3 Scanning system

Corresponding to the block diagram (Fig. 8.1), the scanning system contains the x-ray tube with diaphragm system, the detectors with collimator and the electronics for processing the scanning data.

8.1.3.1 High-voltage generation and x-ray tube

In soft tissue diagnostics, as performed with computed tomography, the differences of the attenuation coefficients relative to the soft tissue structures to be differentiated are of the order of magnitude of percent or even per mil. The error limits for the measured values must have very narrow tolerances and so very high demands are placed on the necessary minimum number of x-ray quanta and their constancy per measured value because of quantum noise. In addition to this, it is necessary to maintain the spectrum of the emitted x-ray radiation as constant and reproducible as possible over the scan time, the exposure time or from pulse to pulse, because of the energy dependence of the attenuation coefficients. A fan-beam apparatus with rotating detectors may operate with pulsed radiation. In this case, imaging is carried out during continuous rotation of the imaging system at intervals of a few angle minutes per projection. The x-ray pulse duration for a five second system can only be a few milliseconds in order to avoid blurring effects.

A whole-body scanner such as the Somatom with its large measurement field and the large object thicknesses which this makes possible requires a slice energy of approximately 30 kWs and a pulse power of the x-ray tube of approximately 40 kW in order to achieve the necessary minimum number of x-ray quanta for an optical focal spot size of 1.6 mm × 1.6 mm. Only an oil-cooled rotary

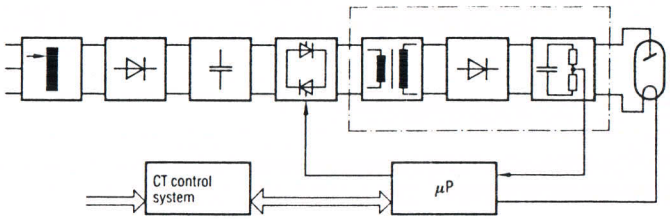

Fig. 8.9 Block diagram of a modern high-voltage generator

anode tube is suitable for this pulse mode. In order to be able to fully exploit the capabilities of a high-speed imaging system, the heat reservoir capacity of the anode must allow the scanning of more than 25 slices (in an uninterrupted sequence). The cooling time until the next series of slices should not significantly interfere with the examination procedure; this is achieved with high-performance oil-air cooling systems. X-ray tubes with a heat capacity up to 3.5 MHU are used.

In scanning systems with constant radiation, i.e. the x-ray tube continuously emits radiation during the entire exposure time, instead of a short x-ray pulse, a sampling frequency of the detectors as high as possible is used in order to again avoid blurring effects. A modern high-voltage generator (x-ray generator) with primary regulation by means of power level compensation and microprocessor control, such as the MIKROMATIC-CT, generates a stable x-ray voltage of 125 kV with a deviation of $< 1\%$ (Fig. 8.9).

The whole-body scanner with continuous rotation uses high-voltage slip rings for transferring the x-ray voltage from the stationary part to the constantly rotating part of the gantry.

8.1.3.2 Measurement system

The detectors and the acquisition system for the scanning data form the measurement system, which converts the x-ray radiation attenuated by the object into a scanning signal suitable for computer input.

To date, three types of detector systems have been used in CT systems:

Scintillation crystals with photomultipliers
Scintillation crystals with photo-sensitive semiconductors
Rare gas ionization chambers

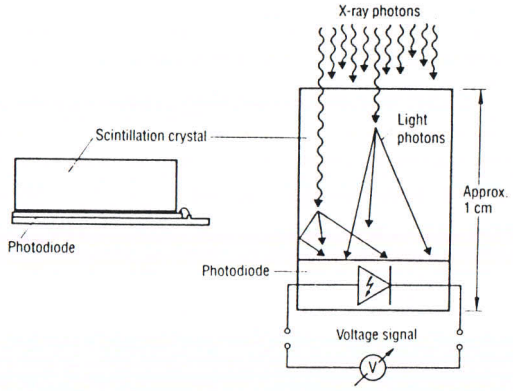

Fig. 8.10
Scintillation crystal with photo-sensitive semiconductor detector

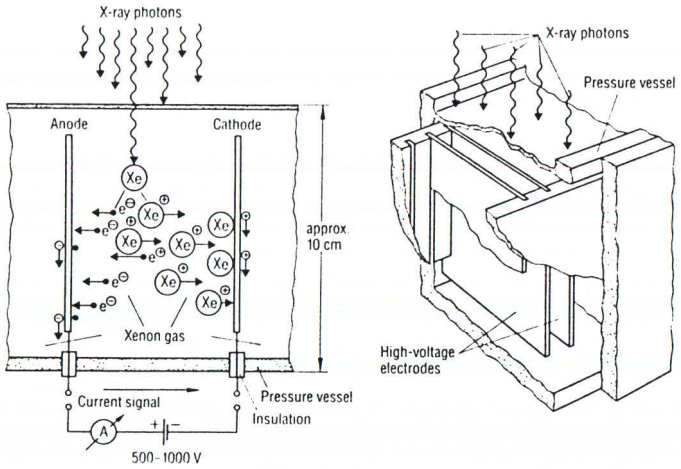

Fig. 8.11 Rare gas ionization chamber detector

Important criteria for the selection of the detector system are good absorption of the incident x-ray radiation and high efficiency in the conversion of the absorbed radiation energy to electrical signals. Naturally, the system must function in a monotonic and stable fashion and cover a large dynamic range. In this case, such crystals as cesium iodide (CsI) and bismuth germanate ($Bi_4Ge_3O_{12}$), with their very high quantum absorption, are more suitable than the rare gases (xenon). However, gas detectors can also be designed for very short decay times, an advantage for an extremely short scanning time. The largest electrical signal combined with a large signal-to-noise ratio for the followup electronics, is provided by the system photomultiplier crystal; however, it does not provide the high packing density of the crystal-semiconductor combination or ionization chambers. Figs. 8.10 and 8.11 show the structure and operation of the semiconductor and xenon detectors. In fan-beam equipment, it is important to position many detector elements as close as possible to each other. On the one hand, radiation losses must be kept as small as possible and, on the other hand, every effort is made to arrange as many elements per solid angle as possible in order to improve the spatial resolution of the system. As a result, the demands on the measurement electronics increase correspondingly, since every detector element must in general have its own measurement channel allocated to it (Fig. 8.12).

In the SOMATOM PLUS the effective number of measurement channels is effectively multiplied by means of rapid electromagnetic deflection of the focal spot of the x-ray tube during the rotation of the system, i.e. every projection is decomposed into several "viewing angles" and thus the resolution capacity of the equipment is increased.

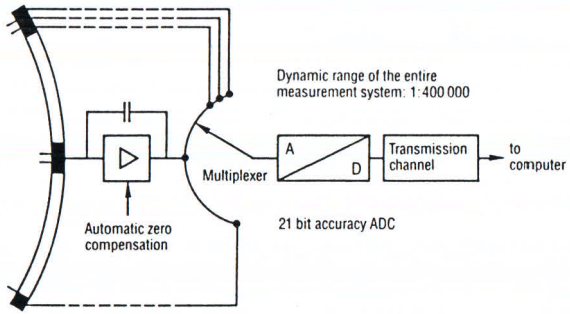

Fig. 8.12 Block diagram of a data acquisition system

The precision requirements of the measurement system follow from the permissible magnitude of the image errors. The point of departure is the radiation dose which can be applied for an image, restricted for a number of reasons, which generates minimum noise in the image. The noise of the measuring equipment must now be kept so small that it no longer makes any additional contribution to the noise in the image.

Thus, high demands are made on the analog amplifier, the integrator and the analog-digital converter, which provides correct computer conversion of the analog measurement values. In order to be able to convert the large signal value range of the analog scanning signal as generated in body images to a digital signal with the necessary high accuracy, converter systems with a resolution of more than 20 bits must be used.

A special technical challenge is noise-free data transmission with continuously rotating systems. Optical transmission systems or slip rings are used here which provide a transmission frequency of up to 200 Mbits/s.

8.1.3.3 Beam path

The beam path and collimating system of the fan-beam machine with rotating detectors can be seen in Fig. 8.13. The collimating system on the tube side is as close as possible to the patient and helps to limit the dose exposure to the necessary minimum for the patient. The lamellar collimator of a crystal detector arranged just above the detector elements and on the focal spot of the tube reduces the proportion of scattered radiation in the measured signal by a factor of approximately 10. This collimator must have an extremely high-precision construction; if the graduation is not equidistant or there is too great a mechanical tolerance, this would immediately affect the image and cause artifacts. Gas detectors are essentially self-collimating due to their electrodes being directed onto the focal spot.
In equipment with a stationary detector ring (ring detector equipment), the elements are directed to the isocenter of the scanning unit. A lamellar collimator therefore cannot be used. Other cylindrical or triangular constructions considerably reduce the radiation utilization.

Thus, only equipment with rotating radiation detector systems provides effective suppression of the scattered radiation, which is the prerequisite for the quantitative evaluation of a CT image.

8.1.3.4 Dose distribution

The dose distribution in the object imaged is quite different in CT systems from that in conventional equipment (Fig. 8.14) [8.1]. Whereas in a conventional x-ray unit, the dose continuously decreases in a ratio of approximately 1000:1

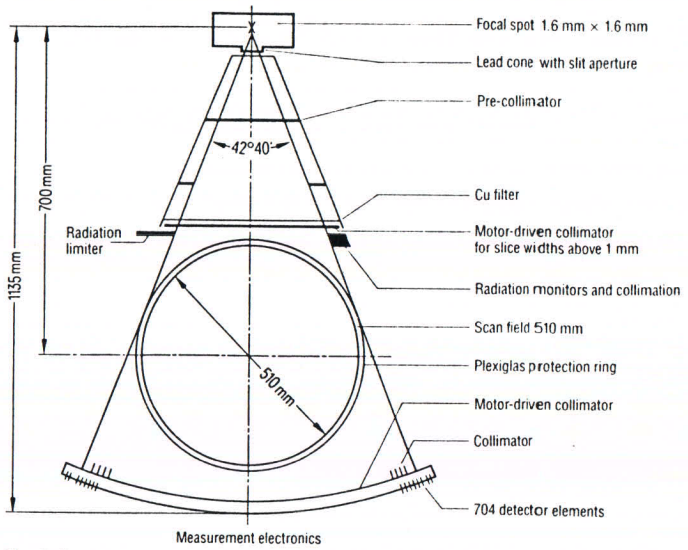

Fig. 8.13
Geometrical arrangement of x-ray tube, collimators and detector system (SOMATOM DRH)

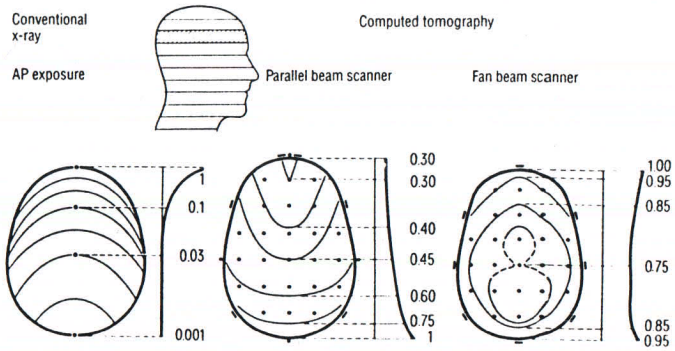

Fig. 8.14
Dose distribution in a conventional exposure with CT images. Imaged with phantom for a typical patient position (relative units)

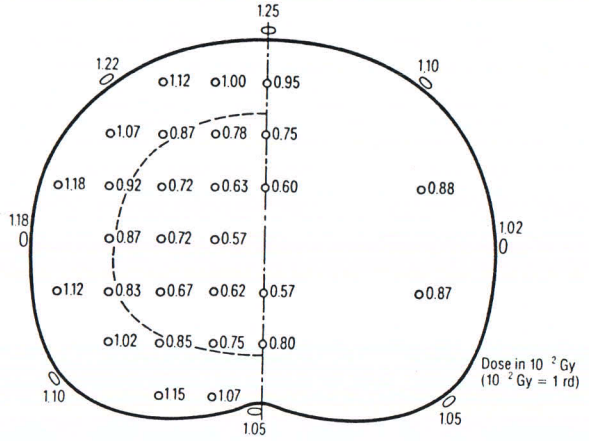

Fig. 8.15
Typical energy dose distribution of the center slice from seven adjacent slices in the liver-pancreas region measured with a fan-beam scanner with the Alderson phantom (disk 24)

going from the side of the body close to the tube to the side of the body far from the tube, in a fan-beam apparatus an almost uniform distribution is measured. The dose distribution in an image of the torso with a fan-beam apparatus can be seen in Fig. 8.15.

8.1.4 Computer system

The mathematical algorithm for CT equipment operating on the parallel or fan-beam principle is very well suited to concurrent image calculation. This is possible using the so-called pipeline principle. For this, the computer is regarded as separated into individual processors, one connected after the other. Each processor performs its own task during the image reconstruction. The processing time of the individual processors is approximately the same. The large number of steps to be performed and the short amount of time available preclude the use of computers commonly found on the market. Special hard-wired computers and chip processors are better suited to the problem. For example, with the SOMATOM it has been possible to make the processing time of a computational step of the same order of magnitude as the projection

sequencing time, i.e. immediately on completion of the measurement process, the image is available in a calculated matrix of 512 × 512 elements (pixels) (Fig. 8.16) and can be displayed in a matrix of up to 1024 × 1024 elements.

Higher ordered control functions of the data processing system, such as equipment control, image display and image storage can be performed by an ordinary minicomputer (host computer). The system is equipped with floppy disk drives, magnetic tape and disk stores and also interactive terminals for inputting patient data, comments and control commands.

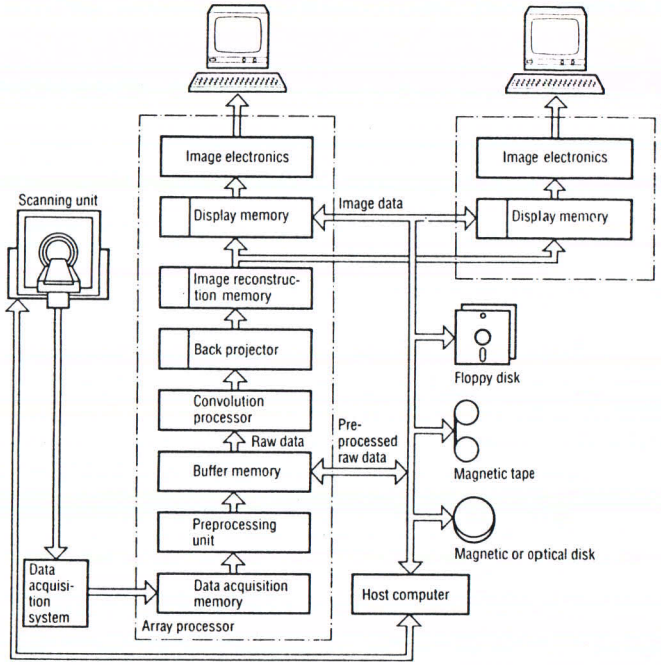

Fig. 8.16 Structure of the computer system

8.1.5 Operating concept

Routine functions such as the selection of scan parameters, exposure release, image recall and table feed are usually performed at an operating console (Fig. 8.17). A user-friendly system characterized by software-controlled dialog, menu-driven commands and only a few input elements to operate minimizes errors and provides a fast scanning sequence, thus ensuring a high patient throughput.

If the operating console is attached to its own image store, then after an image has been transferred to this store the computer is free for another scan and the observer can select the image representation which seems correct to him for diagnosis without any delay.

Every pixel of the calculated image is represented in the image memory by digital values. In order to display this information on the viewing monitor,

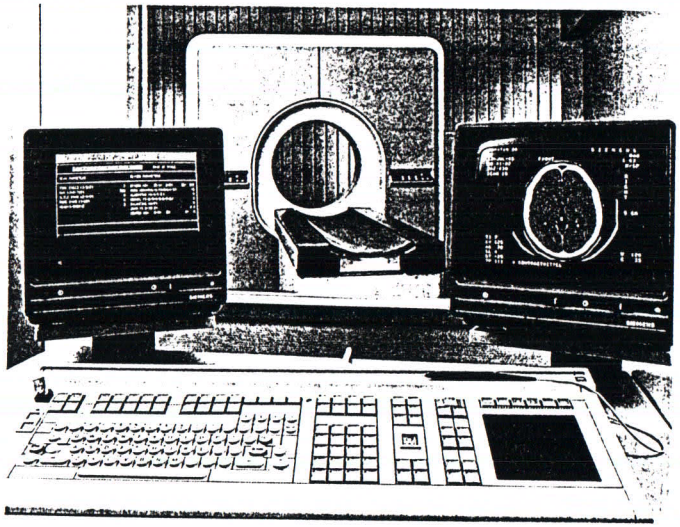

Fig. 8.17
One of the many functions of the CT system control console with the SOMATOM is to vary window position and width of the images displayed

it must be read out from the memory synchronously with the video sync signal. Every bit combination then has a signal amplitude allocated to it through a digital-analog converter, which in turn controls the brightness of the television image tube. Modern systems operate with high frame rates and more than 1200 lines per frame.

Of course, a computer-controlled operating concept is flexible enough that new scanning techniques and evaluation functions, as well as extensions and expansions to the CT system, can be implemented [8.2].

8.2 Image display, documentation and evaluation

8.2.1 Image display

For the morphological evaluation of a CT image, it is necessary to focus on the essential information for a given examination. The information inherent in the CT image lies in the absorption range between −1000 and approximately +3000 HU (Hounsfield Units, i.e. CT values). The absorption values of the CT image are therefore converted to gray levels and displayed on a viewing monitor. In an ideal case, the eye can distinguish approximately 100 brightness graduations in a television image, but under normal working conditions not much more than 30.

The user could thus never distinguish between the approximately 4000 values comprising the entire range of CT values. Furthermore, the observer is often only interested in a small section of the absorption range, e.g. the differentiation of gray and white brain matter, which only differ by approximately 10 CT values.

In order to display small absorption differences, so-called *image windowing* is therefore used. Here, only a part of the CT scale is selected and spread over all brightness values between black and white. Even small absorption differences inside the selected window are displayed as distinguishable gray tone differences, while all CT values below the window are displayed black and CT values above the window are displayed white.

Since the position and the width of the window can be varied at will, several different medical questions can be answered from the same CT image, depending on the window selected. Typical applications here are images in the heart-lung region and the optional display of soft tissue and bone structures.

If a linear gray scale is used for the display, this leads to a compression of the dark gray tones due to the distortion of the television tube characteristic. This favors differentiation between details, because, due to the physiology of the eye, gray tones can be more easily recognized in the dark parts of the image than gray tones in the bright parts of the image with the same differences in illumination density.

In order to improve the recognizability of the gray tone image, an additional distortion of the image is often also used in the form of look-up tables. Here, a fundamental distinction can be made between two applications:

- A distortion with the help of a look-up table *before* windowing can be used in order to spread out or compress specific CT-value ranges specific to an organ, e.g. in order to optically magnify the interval between the gray values of white and gray brain matter.
- A distortion with the help of a look-up table *after* windowing can be used in order to compensate for the effects of the blackening curve specific to the film when the CT image is recorded onto x-ray film.

In general, it can be said that apart from other factors such as dose, detector arrangement and reconstruction algorithm, considerable importance should be attached to the imaging system which, together with photographic documentation, represents the last component in the CT system imaging chain. Here, only a few key words will be mentioned, such as video bandwidth, modulation transfer function and flicker-free displays. Today, the dimensioning of the CT imaging system is normally based on display in a 512 × 512 matrix, where it is unimportant for the image system whether this display matrix has been directly calculated or has been produced by interpolation.

8.2.2 Image documentation and archiving

After the CT image has been displayed on the viewing monitor and a diagnosis has possibly been made, the question arises as to the documentation of the examination result and the archiving of the image material. These requirements take up a considerable proportion of the time spent in routine operations.

Depending on the nature of the CT image, image documentation and archiving can be divided into two methods:

- Photography: window position and width must be defined before exposure, all information outside the selected window is lost.
- Digital image storage: the entire information content of an image is kept; a specific image setting can be reproduced at any time or the image can be evaluated numerically based on latest findings.

For the foreseeable future, these two methods should be regarded as complementary and not competing.

8.2.2.1 Photography

Legally, the CT image should be regarded as an "image from an x-ray examination". This means that the law requires images to be safely stored for many years. Although the image in the form of a photographic document can clearly show the relevant information for the findings, the window selected may be completely unsuitable for other medical questions.

However, photographic documentation is certainly the most important type of long-term archiving at the present time. Multiformat cameras (see section 7.2.9) are available for this purpose. They allow to a large extent any subdivisions of the transparent film from large format to slides. Film magazines, which eliminate the need for frequent changing of the film cassettes, greatly simplify the operation of this equipment. A further step in the automation of photographic documentation is the direct connection between multiformat camera and developing machine with wet development in a 90 second process.

The software provides additional support functions for image documentation: image and patient data, evaluation results, as well as marker arrows and comments, can be superimposed. The layers examined can be marked in a Topogram for orientation. A characteristic which can be freely defined for the camera monitor enables the optimization of image results.

The digital camera, i.e. the so-called laser camer, only recently introduced to the market, represents a further advance in camera technology. With this type of camera, the image is not photographed from a monitor. Instead, the gray values of the pixels are transferred in digital form to the camera and directly control the exposure time for every individual pixel. The result is enhanced imaging accuracy and increased image dynamics. Today this type of camera is mainly used in upper class CT-systems. Special interfaces had to be developed for the CT scanning system to allow the digital transmission of images to the camera in a matter of seconds in order to provide the same operating speed as with conventional multiformat cameras.

8.2.2.2 Digital image storage

Digital image storage usually takes place onto magnetic tape or floppy disk (see section 7.2). However, this type of image storage has lost importance as a routine method of documentation with the increasing size of the matrix of the images. Even when coding procedures are used for reducing the redundance or when reduced matrix sizes are stored, the capacity of magnetic tape and in particular of floppy disks is inadequate or the costs per stored image are high. Further limiting factors, such as poor access to the images and limited lifetime of the data storage media – usually only a few years without resorting to exceptional measures – must also be considered.

However, this situation is considerably improved when another storage medium is used, the digital optical disk (see also section 7.2.2). With this data storage medium, the image information is burned in in digital form by means of a laser beam; it can then no longer be erased.

Optical disks provide a very high storage capacity (several thousand images per disk). This means low costs per image and in addition a long lifetime for the data storage medium. No special maintenance procedures are necessary for a period of at least 10 years.

Optical disks accommodated in so-called juke boxes, with direct access to a large number of disk cassettes, will in the future form the long-term archives of PACS systems.

PACS (Picture Archiving and Communication Systems) is the corner stone for a future x-ray department without film, in which all imaging systems are connected via fast data lines to a digital image archive from which the doctor can rapidly access every image in its original digital form.

8.2.3 Image evaluation

In recent years, certain evaluation procedures for CT images have emerged as useful aids for the doctor. However, none of the procedures can take away the doctor's responsibility in making his diagnosis. Only the tools are provided, to be used for answering certain diagnostic questions.

An image processing system is needed to perform the image evaluation. Usually one of the following three systems is used:

- The standard operating console of the CT system in departments with low numbers of patients, where imaging and evaluation can be carried out alternately;
- An additional evaluation console, connected to the computer system in the same way as the operating console and therefore allowing access to all peripheral image stores and to the image processor of the system;
- An independent evaluation console with its own computer, to which the images are either transferred by magnetic tape or floppy disk or to which they are directly transferred from the CT system by a data link.

The evaluation procedures themselves and the capabilities of the evaluation system can be roughly divided into two categories:

- *Subjective evaluation* procedures in which the doctor displays or prepares the images in a suitable form for making his diagnosis;
- *Objective evaluation* procedures in which the values of the image matrix are used directly for measurements or calculations and the results give information on the relevant diagnosis.

8.2.3.1 Subjective image evaluation procedures

These procedures include:

Image display with suitable look-up tables
Multi-window image display
Multiple image displays
Image subtraction
Image filtering
Image magnification
Profile section
Reconstruction of reformatted images
3-dimensional image display

Reference was made to image display with suitable look-up tables in section 8.2.1. A special case of a non-linear gray scale is the highlighting of density regions selected by the user. This makes it easier for him to find certain diagnostically relevant areas.

Image display with several windows makes it possible either to display a small density region with maximum contrast inside a body displayed with a large window or, in images with large differences in density, to display different regions with optimum contrast at the same time.

Multiple image displays make it possible to display several consecutive layers of an organ in order to produce a 3-dimensional impression.

A method often used for operational checks and contrast examinations is the comparison of two CT images. The difference can be seen after subtraction of the images. This method is limited by the spatial reproducibility of two images separated in time.

2-dimensional filtering of images is a well-known method for smoothing images or enhancing contours. In the first instance, image filtering is carried out by using a corresponding convolution kernel during image reconstruction. Subsequent image processing has usually only an additional cosmetic effect.

In order to improve the recognizability of an image detail, it can be enlarged with the help of image magnification. However, magnification does not produce any extra gain in information.

Small density differences can be more easily identified without selecting too narrow a window, which would increase the image noise, by using the profile section; the CT values are then plotted as a curve over the section of interest.

By suitable choice of the gray scale in displaying the section, even small density differences can be unambiguously differentiated.

One of the main advantages of a series of digitally processed transverse slice images, which together form a cube of CT values, is the possibility of reconstructing images with any orientation, i.e. reformatted images. Of special impor-

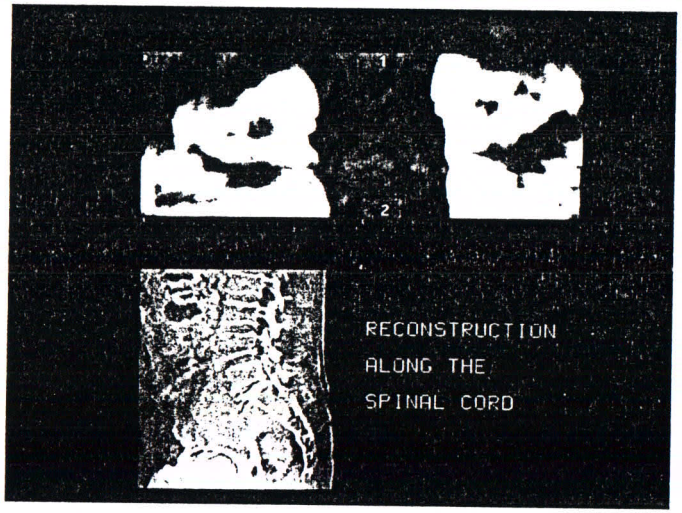

Fig. 8.18
Reconstruction of a curvilinear reformatted image

tance here are sections which are perpendicular to the original transverse sections and which thus give a quasi "technical" representation of the object of interest. In images of the skull and the spine, computer simulation of highly inclined positions of the scanning unit are also of great importance. Curved sections, e.g., along the spine, can also help in spinal examinations (Fig. 8.18). Even completely freely defined slice planes, e.g. through three marked points in different slices, are useful in the abdomen for certain diagnostic questions, although it is then often difficult to obtain a good spatial impression [8.3, 8.4].

The same cube of CT values can be used for calculating 3-dimensional images (Fig. 8.19). A special problem in the calculation of such images is the determination of the contours, which can only be automated at clearly defined boundaries, e.g. at the skin surface or at the edges of bones. The differentiation of soft tissue can still only be done manually and is therefore extremely time consuming.

However, the calculation of 3-dimensional images, e.g. in plastic surgery and in general in planning operations, is gaining in importance.

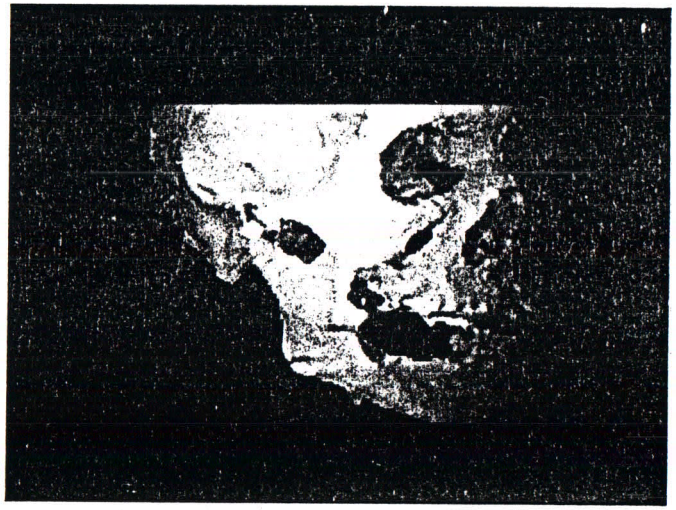

Fig. 8.19
Three-dimensional reconstruction of the cranial bone surface from a sequence of transverse CT images

8.2.3.2 Objective image evaluation procedures

These include:

- Distance and angle measurements
- Evaluation of area, volume and average density in regions of interest
- Symmetry comparison
- Histogram

The most important and the most frequently used evaluation function is the measurement of distances and angles in the image. Here, the fact that the CT design principle ensures perfect reproduction with no distortion is exploited.

Since the computational accuracy is limited by the pixel size and the accuracy with which the user sets a measurement point, it is recommended when measuring small objects to first magnify the corresponding image section.

There are many different ways of evaluating regions of interest (ROIs). The most important determinations are for the area, the volume or the average

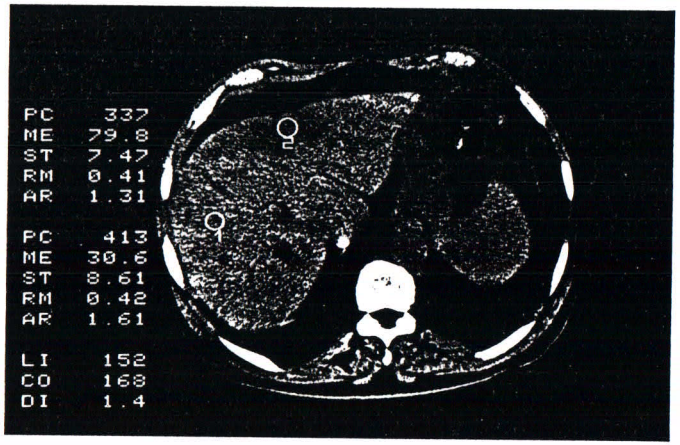

Fig. 8.20
Comparison of the average absorption values over two regions of interest
Region 1: 79.8 HU, normal tissue
Region 2: 30.6 HU, tumoral tissue

density of a region. Here, the ROI can itself be in the form of a point, a circle or any arbitrary shape (Fig. 8.20).

It is often necessary to compare two regions in the image with each other. A special case is that of symmetry comparison in the skull region, where the two regions to be compared are reflected about a selectable line of symmetry. In calculating the average density over an ROI, the standard deviation of the result is also usually calculated; this gives information on the variance of the density value. If one is interesterd in the exact distribution of the density values over the ROI, a histogram of the density values gives information on the internal composition of the ROI.

8.2.4 Applications

Special applications were already developed very early in CT. Some of these, e.g. dynamic computed tomography, have in the meantime become standard procedures. Other procedures are still under development or work in progress. Here, we will give a brief description of the most important special applications which are known today.

Evaluation of dynamic image series after contrast medium injection

CT scanners with short scanning times, high imaging frequencies and short delay times between image acquisitions make it possible to display fast physiological processes within a slice through the body. This permits the exact differentiation of lesions from the enhancement phase of a contrast bolus, e.g. in order to dispay vessel changes or the arterial and capillary phase in parenchymatous organs. Such a series of images is evaluated quantitatively by numerical determination of the density changes in the ROIs over time and displaying them in the form of curves (Fig. 8.21). Special programs are available to help in interpreting the density curves, e.g. for curve smoothing or calculating a gamma fit. Other possibilities of assessing the contrast dynamics are so-called parameter images or, often much more impressive, the display of the contrast medium enhancement by a sequence of images shown at real-time speeds on the image monitor [8.5, 8.6].

Evaluation of dynamic image series after xenon inhalation

In measurement of the brain blood flow by Dynamic CT, the patient inhales a mixture of stable xenon gas and oxygen or air over a period of several minutes. At the same time, CT images of selected layers of the brain are acquired. The time between the precontrast images and the corresponding contrast images is exactly measured together with the arterial xenon concentration. With the help of special programs, the regional cerebral blood flow and the xenon lambda coefficient (a tissue parameter which indicates the relative solubility of xenon) can be calculated from the measured data and the images. These values are displayed as so-called flow and lambda images (Fig. 8.22). Flow values are usually given in milliliters per 100 g brain tissue. Lambda values indicate the ratio of brain tissue to blood and are therefore dimensionless [8.7].

Evaluation of ECG-triggered cardiac images

ECG-triggered cardiac images can be obtained from a sequence of CT images in which the ECG information is plotted together with the scan data. In order to make the data acquisition more effective, the individual images are initiated at different times relative to the cardiac phase.

A program sorts the scan data for the desired cardiac phase and calculates the associated image. From a sequence of such images, the movement of the heart can be displayed in real time on the monitor [8.8].

CT image for biopsy and stereotaxy

The CT image can be used in a routine manner as the basis for biopsies and stereotactic interventions, because it provides a perfect 3-dimensional assign-

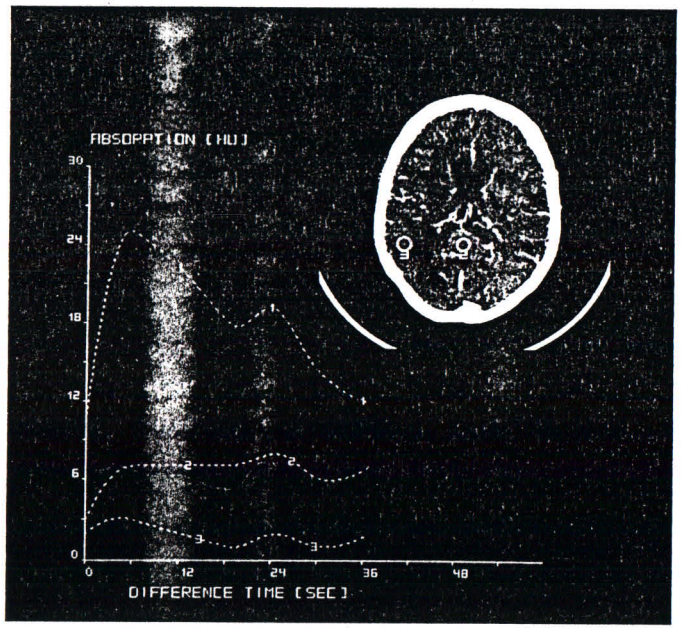

Fig. 8.21
Evaluation of the contrast medium distribution over time for different regions of the cranial slice displayed

Region 1: Vessel during contrast medium enhancement
Region 2: Tumor
Region 3: Normal tissue

ment of every pixel. It is particularly helpful when other methods, such as ultrasound or fluoroscopy, cannot display with sufficient precision the target volume or the structures endangered by the needle, lying between the incision point and the target volume. In these examinations, the patient is usually fixed in a stereotactic frame which defines a system of coordinates.

Programs can then be used to calculate the coordinates for the target apparatus after marking the incision and target points in the CT image [8.4].

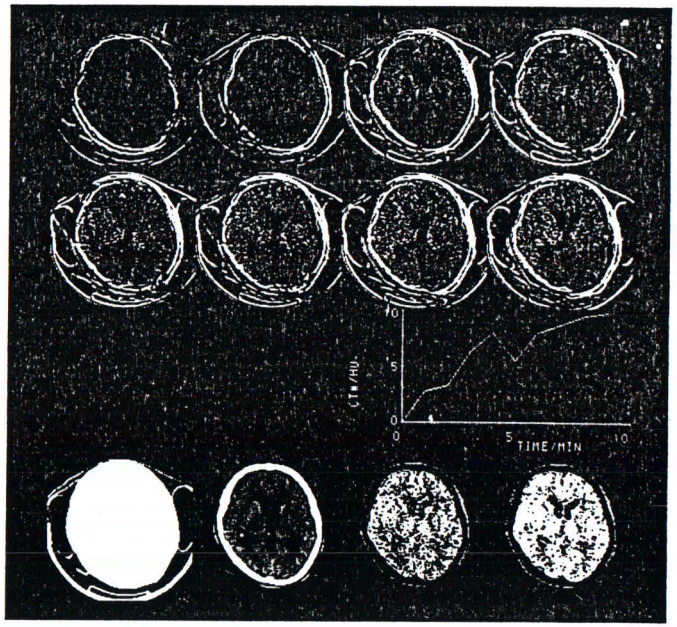

Fig. 8.22
Xenon contrast study. The top eight sections are subtraction images taken from a dynamic series. The bottom four figures show, from left to right: mask (scaled for higher accuracy and thus located outside the window), unsubtracted CT image, flow image and Lambda image. In between, diagram of contrast medium enhancement for a point marked in the CT image.

Generation of images from the dual energy method

CT images represent the linear attenuation coefficients for the volume elements of the imaged layer, but in no way are they images of the density as is usually asserted incorrectly. The linear attenuation coefficient is a product of the capacity for x-ray attenuation and the local density. If, for example, there is a lung node showing increased CT values in the image, then it is not certain whether

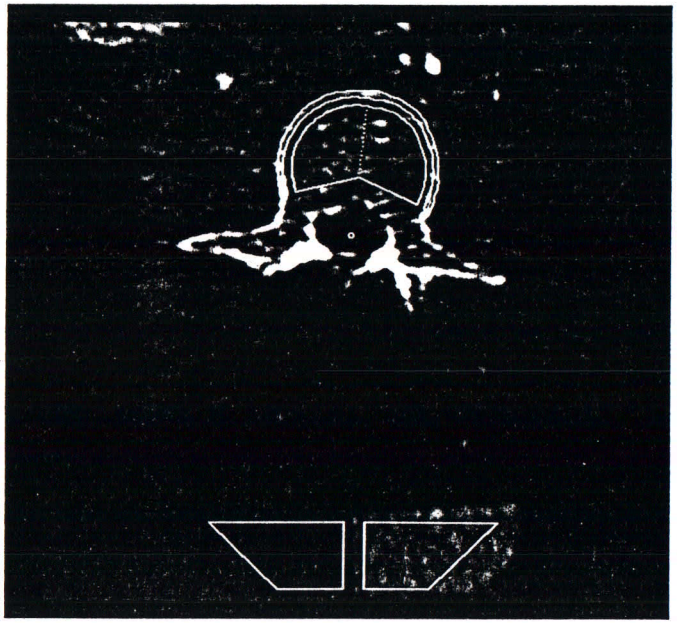

Fig. 8.23
Determination of bone mineral content. Here, the evaluation of a calcium density image from a dual energy measurement. Automatic contour finding for regions of interest (ROIs)

Top: cortical ROI, spongy ROI with symmetry axis, center of gravity of ROI through spinal cord

Below: reference materials for calcium equivalent (right) and water equivalent (not visible in the calcium density image)

the reason for this is diffuse calcification, i.e. elements with a higher atomic number, or a fibrosis, i.e. an increase in the density [8.9].

The image of a layer with two different spectra makes it possible to calculate images of the density distribution of specific materials with suitable programs instead of the usual CT images, e.g. so-called soft tissue images and bone images. Based on these, electron density images and so-called mono-energetic CT images can be reconstructed. The advantage of the latter is that artifacts caused by spectral hardening of the x-ray radiation are eliminated (e.g. the Hounsfield bars in the posterior cranial fossa).

Determination of the mineral calcium content in the vertebrae

In order to determine the mineral calcium content in vertebrae, the center of vertebrae L1 to L3 is imaged for each CT scan, with reference materials measured at the same time, e.g. embedded in the patient couch. With suitable software, the calcium content of the vertebra can be calculated in calcium equivalence units by means of ROI evaluation of the measured bone structures and the reference materials, assuming that computer assisted contour determination is available (Fig. 8.23) [8.7, 8.10].

The CT image in radiation therapy planning

The CT image directly provides important information for optimal radiation therapy planning. On the one hand, this involves information on the size and volume of a lesion and its topographical and anatomical relationship to neighboring structures and, on the other hand, information on the density of the structures which can be taken into account in the planning process.

The planning process results in the radiation plan and its local dose distribution, which can be directly superimposed on the CT image in the form of isodose curves.